Univerzita Karlova v Praze
Matematicko-fyzikální fakulta

BAKALÁŘSKÁ PRÁCE

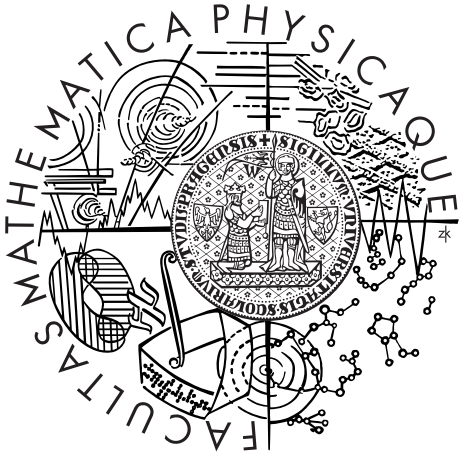

Zdeněk Rafaj

Studium adsorpčních vlastností oxidovaného povrchu slitiny TiNb optickými metodami

Katedra fyziky povrchů a plazmatu

Vedoucí bakalářské práce: doc. RNDr. Václav Nehasil, Dr.

Studijní program: Fyzika

Studijní obor: Obecná fyzika

Praha 2015

Charles University in Prague
Faculty of Mathematics and Physics

BACHELOR THESIS

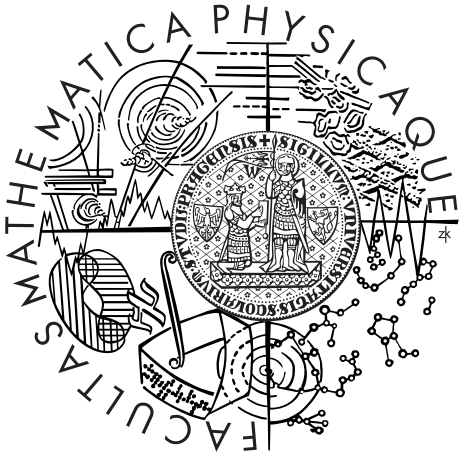

Zdeněk Rafaj

Surface oxide on the TiNb alloys — optical study of adsorption properties

Department of Surface and Plasma Science

Supervisor of the bachelor thesis: doc. RNDr. Václav Nehasil, Dr.
Study programme: Physics
Specialization: General physics

Prague 2015

I would like to express my sincere gratitude to my supervisor doc. RNDr. Václav Nehasil, Dr. for his advise, for his patience and especially for the time he spent discussing the topic. I wish to gratefully acknowledge RNDr. Viktor Johánek, Ph.D. for granting access to the infrared instrument and his support during the measurements and RNDr. Ivan Jirka, CSc. for a preparation and a provision of TiNb samples.

I declare that I carried out this bachelor thesis independently, and only with the cited sources, literature and other professional sources.

I understand that my work relates to the rights and obligations under the Act No. 121/2000 Coll., the Copyright Act, as amended, in particular the fact that the Charles University in Prague has the right to conclude a license agreement on the use of this work as a school work pursuant to Section 60 paragraph 1 of the Copyright Act.

In ..... date ..... signature of the author

Název práce: Studium adsorpčních vlastností oxidovaného povrchu slitiny TiNb optickými metodami

Autor: Zdeněk Rafaj

Katedra: Katedra fyziky povrchů a plazmatu

Vedoucí bakalářské práce: doc. RNDr. Václav Nehasil, Dr., Katedra fyziky povrchů a plazmatu

Abstrakt: Mezi nejrozšířenější materiály pro kloubní náhrady patří slitina Ti-6Al-4V obsahující toxické prvky Al a V. Jako slibná náhrada se jeví netoxická slitina TiNb. Jelikož není TiNb doposud dostatečně popsán, zaměřuje se tato práce na charakterizaci povrchu (metodami XPS a FT-RAIRS) vzorků po ošetření H_2O a NaOH u přírodně (na vzduchu) a tepelně (1h v 600°C) zoxidované slitiny. Po přípravě je povrch tvořen oxidy TiO_2 a Nb_2O_5. Po zahřátí vodou ošetřeného vzorku je vidět výrazná redukce. Jen slabá redukce nastává u vzorku po úpravě NaOH. Toto chování lze vysvětlit tvorbou tenké povrchové pasivační vrstvy. Tepelně připravený oxid zůstává po všech procedurách beze změn. IR spektroskopie neprokázala přítomnost OH^- skupin, které jsou významným indikátorem biokompatibility u materiálů určených pro kloubní implantáty.

Klíčová slova: slitina TiNb, OH skupiny, biokompatibilita, XPS, FT-RAIRS

Title: Surface oxide on the TiNb alloys — optical study of adsorption properties

Author: Zdeněk Rafaj

Department: Department of Surface and Plasma Science

Supervisor: doc. RNDr. Václav Nehasil, Dr., Department of Surface and Plasma Science

Abstract: Contemporary commercially used bone implants include a Ti-6Al-4V alloy. Due to the toxicity of aluminum and vanadium, a TiNb alloy with non-toxic elements appears to be a promising replacement. However, only limited information about this alloy is available. This study investigates TiNb surface by XPS and by a complementary method FT-RAIRS. Two sets of samples were prepared. One was only polished and spontaneously oxidized in the air (natural oxide), the other one was thermally oxidized (1h at 600°C) after the polishing. Two samples of each oxide were treated either with H_2O or with NaOH. It was found that after the preparation both samples (a natural and a thermal oxide) are in highly oxidized states TiO_2 and Nb_2O_5. In case of the H_2O treated natural oxide, these oxidation states are reduced by heating. Only small reduction after NaOH treatment is observed. This behavior is explained by a thin layer of Ti and Nb oxides. Thermal oxide seems to remain without changes during all procedures. IR spectroscopy does not prove an OH^- groups appearance which is important for biocompatibility of a bone implant.

Keywords: TiNb alloy, OH groups, biocompatibility, XPS, FT-RAIRS

Contents

1. Introduction

1.1 Biocompatibility and Surface Science

Nowadays, modern technology effects our lives at every moment. One of the most important areas which have a major role in our lives is medicine. A progress in the material science achieved especially during the last decades helps us to perform procedures improving and saving human lives. This thesis is focused on a part of medicine including a use of implant devices in the human body. Materials suitable for long-term implants are called biomaterials. For these materials, there are several conditions required to ensure their safe use in human body. The fulfillment of these conditions depends on the surface structure of an implant.

A mutual co-existence of a biomaterial and a living tissue is crucial. The co-existence needs to be achieved without damaging the body. We call that biocompatibility. Biocompatibility is closely connected with implementable devices. During the time between the years 1940 and 1980, it was shown that a choice of highly chemically unreactive substances leads to increase of biocompatibility. Hence, it results in a use of stainless steel, strongly passivated cobalt-chromium alloys, titanium alloys, polymer PTFE, PMAA, polyethylene or silicons [1]. However, there are some special applications where the specific body response to implant materials is required, e.g., apatite formation at the interface between a bone and a bone implant [2].

In fact, the most biological reactions occur at surfaces and interfaces [3]. As it was mentioned before, not all materials are suitable for being implanted onto a tissue. The use of these materials can trigger a body defense mechanism which leads to an inflammatory response [4]. The inflammatory response starts with protein adsorption at the surface [5]. The great importance of a surface structure is for all these reactions indisputable.

The biomaterials that we know from a current practice were introduced in the late 1940s [3]. Since then, new methods of studying and modifying materials were developed. That all had a considerable impact on a progress of biology and medicine. A detailed understanding of the role of surface science allows us to reduce complex processes into elemental steps. In case of bone implants, we can only investigate the hydroxyl groups formation which is a part of the process of growing a material and a bone together [6].

Surface analyses provide us information about surface composition, chemical state of compounds or its orientation. The information is used to determine certain properties of the material. After a comparison of results with similar experiments, we can derive the properties of the measured material. That is especially useful in case we search for a particular quality, i.e., hydroxyl groups formation.

1.2 State of the Art

Nowadays, titanium alloys are used extensively for dental implants, femoral stems, pacemaker cans, heart velves, fracture plates and spinal cages [1]. For these biomedical applications, one of the most common alloys is Ti-6Al-4V. It has a lot

of desired properties, i.e., low modulus of elasticity, fatigue strength, corrosion resistance and biocompatibility [7].

However, there are studies which show that the presence of aluminum and vanadium can harm human body [8, 9, 10]. Replacement of these elements is an important task considering that the materials are designed for long-term use. The toxicity of these elements lies in corrosion processes. All metallic implant materials corrode. The amount of the released material during the corrosion is small but it is significant in comparison with concentrations of metallic components in a human body. Products of this corrosion are biologically active which brings possible risks. The result effect depends on a particular element. Aluminum and vanadium belong among elements with negative effects. For instance, aluminum rich neurofibrillary tangles were found in bodies of patients with Alzheimer's disease [11]. The possible replacement can be found in Nb, Ta, Zr, Mo and Sn which are considered as the non-toxic elements [10].

Titanium-niobium (TiNb) alloy appears to be promising replacement of Ti-6Al-4V. TiNb has attractive properties for implant material, i.e., lower modulus of elasticity than Ti-6Al-4V, low density, good fatigue strength, corrosion resistance, and it fulfills the conditions for biocompatibility [12]. In the context of biocompatible use, there is not much information available concerning this alloy.

Due to the common use of Ti-6Al-4V, the apatite formation process has been in the interest of many studies [2, 6, 13]. Thus, it is a well-described phenomenon. Titanium is a bioinert material. That is important for biocompatibility but it also prevents from a bone growth which is, in this case, a wanted process. The growth of bone and implant material together improves the fixation of implant. Therefore, other ways of a growth initialization are used, e.g., porous titanium coating. After the porous structure is created, the bone can grow into it and provide the necessary fixation of the implant.

The process of a bone growth at a surface of an implant can be observed *in vitro*. Due to the understanding of involved processes, we can focus on only particular parts of them, e.g., the -OH groups creation. The whole procedure consists of the porous structure preparation, which can be done by sintering or plasma spraying titanium at a titanium alloy (Ti-6Al-4V) substrate [6]. This structure itself provides better conditions for the apatite growth process. The affect can be improved by using different means of a surface treatment. After porous layer formation, we soak it in the NaOH aqueous solution. There are possible modifications during and after the soaking procedure such as the choice of an appropriate temperature. It results, in appearance of a sodium titanate hydrogel layer. The layer of sodium titanate increases the amount of Ti-OH groups. During the NaOH treatment the -OH reacts with the titanium oxidized surface which is described by the equation 1.1. -OH groups bonding at the titanium surface are the first step in the apatite growing process.

$$TiO_2 + OH^- \rightarrow HTiO_3^- \tag{1.1}$$

Besides the reaction in equation 1.1, other reactions can simultaneously occur. These reactions are shown in equations 1.2, 1.3, 1.4 and 1.5.

$$Ti + 3OH^- \rightarrow Ti\,(OH)_3^+ + 4e^- \tag{1.2}$$

$$Ti\,(OH)_3^+ + e^- \rightarrow TiO_2 \bullet H_2O + 0.5H_2 \uparrow \tag{1.3}$$

$$Ti\left(OH\right)_3^+ + OH^- \leftrightarrow Ti\left(OH\right)_4 \tag{1.4}$$

$$TiO_2 \bullet nH_2O + OH^- \leftrightarrow HTiO_3^- \bullet nH_2O \tag{1.5}$$

These procedures are followed by immersion of the samples into the simulated body fluid (SBF). SBF is a solution designed to simulate human blood plasma, i.e., blood without red blood cells. It is the liquid with the similar ion concentration and the same pH value. The solution has the same temperature as a human body for the time of a samples soaking. This emulates the human body environment and can lead to the desired apatite formation at the surface. The apatite formation process is described by a series of reactions shown in equations 1.6, 1.7 and 1.8.

$$HTiO_3^- + Ca^{2+} \rightarrow CaTiO_3 + H^+ \tag{1.6}$$

$$3CaTiO_3 + 2PO_4^{3-} + 6H^+ \rightarrow Ca\left(PO_4\right)_2 + TiO\left(OH\right)_2 \tag{1.7}$$

$$2Ca\left(PO_4\right)_2 + 4Ca^{2+} + 2PO_4^{3-} + 2OH^- \rightarrow Ca_{10}\left(PO_4\right)_6\left(OH\right)_2 \tag{1.8}$$

When the NaOH treated samples are immersed in SBF, the Na^+ ions are exchanged with H_3O^+ ions which increases the Ti-OH groups concentration. These negatively charged OH^- groups interact with Ca^{2+} ions in SBF. Ca^{2+} ions accumulate at the surface and bond with negatively charged phosphates in SBF. The result is an amorphous calcium phosphate formation. This form of calcium phosphate spontaneously changes into apatite, the more stable phase in an SBF environment. *In vivo*, this process means that the artificial material bonds to the living bone via bonelike apatite.

1.3 Thesis Goals

The goal of this thesis is to characterize the surface structure of the TiNb alloy and to describe changes in the surface consistence after different kinds of sample treatment procedures, eventually to find general patterns in the behavior of these processes which are applicable for the TiNb alloys, and that all to compare with processes which are necessary for biocompatible bone implant materials.

The surface characterization includes an investigation of surface oxidation process, i.e., the consistence of particular oxidation states depending on different treatment procedures, eventually the oxides stability. The goal is also to determine surface changes after different surface treatments. The treatment procedures are boiling in H_2O and NaOH. The surface structure will be discussed with respect to the surface structures of biocompatible materials which are used for bone implant needs.

Because this alloy is intended to be used as a possible future bone implant material, the surface analyses will be focused on this research area, i.e., a presence of OH^- groups bonded at samples surfaces. The result of this thesis will be also a comparison of these groups appearance after particular phases of samples treatments.

2. Analysis Methods

2.1 XPS

The dominant sample analysis method used in this thesis is X-ray photoelectron spectroscopy (XPS). XPS is a qualitative and quantitative analysis of a surface element composition. This technique is based on the photoelectric effect explained by Einstein in 1905 (the Nobel Prize in Physics in 1921). XPS, also called ESCA (Electron Spectroscopy for Chemical Analysis), is used for determination of surface element concentrations and identification of element chemical states [14]. The knowledge of chemical states can be used to derive chemical compounds present in the top layer of surface or adsorbed on the surface.

A spectrometer consists of an X-ray lightsource, a measured sample and an electron kinetic energy analyzer. The XPS measurement starts with a generation of an X-ray light. This light irradiates a measured sample. The X-ray photons can penetrate many micrometers into the sample and interact with its atoms. The energy of X-rays is high enough to ionize the atoms. The ionization means that the incident photon is absorbed by an electron from the principal electron energy level of an atom. The electron uses the absorbed energy to liberate itself from the atom and the rest of the energy is transformed into the electron kinetic energy. Then the atom is depleted of the electron, it is ionized, and finally the electron is free. These electrons are quickly slowed by electromagnetic field of other atoms. Thus, only electrons from a few top atomic layers leave the sample and are detected. The process, in which atom absorbs a photon and emits an electron, is called a photoelectric effect. The overall process can be described by the equation 2.1 [15].

$$E_K = h\nu - E_B - \phi \tag{2.1}$$

The equation 2.1 represents the law of conservation of energy for this system. E_K is the electron kinetic energy. It obtains this energy by absorption of a photon energy $h\nu$ where h is the Planck constant and ν the light frequency. A part of this absorbed energy is used to overcome the binding potential represented by binding energy E_B. If the sample is a conductor in contact with spectrometer, we will denote by ϕ the work function of the spectrometer and E_B is relative to the Fermi level. Insulators do not have as well-defined Fermi level as conductors and it is difficult to ensure electrical contact with the spectrometer. In case of insulating samples we will designate a value by ϕ which also includes the sample surface potential and reference point for the binding energy E_B. In comparison to spectra acquired from different insulating samples, it is important to found a common reference points.

The equation 2.1 gives us a relation between binding and measured kinetic energies. The result of an XPS measurement is a spectrum (a plot) which shows counts of detected electrons against their binding energies. The spectrum has characteristic peaks corresponding to the core levels of electrons within an atom, i.e., 1s, 2s, 2p, 3s, etc. Core levels of atoms of different elements have different energies. Therefore, the binding energy is an unique value for different elements and different states depending on bonds between atoms.

All parts of XPS requires ultra high vacuum (UHV) conditions with the pres-

sure lower than about 10^{-7} Pa [15]. It is particularly due to a need for a preservation of the clean surface during an *in vacuo* experiment and an analysis. Because the contamination comes from the gas molecules in the vacuum chamber, the pressure directly effects the amount of adsorbates at the sample surface.

The first part of the spectrometer is the lightsource. Probably the most common lightsources generate a non-monochromatic X-ray. They use the Kα characteristic radiation emitted from Al or Mg anode. The device for generation of X-ray radiation is called an X-ray tube. It is basically a vacuum tube. Electrons are emitted from the heated cathode due to the high voltage between the cathode and the anode (a few kV). Emitted electrons are accelerated to the anode by the electric field. After electrons reach the anode, two possible scenarios happen. First, some electrons are scattered by strong electric field of atom nuclei. During the scattering, the electrons emit (Bremmstrahlung) an X-ray radiation with a continuous frequency spectrum. Second option is that the incident electrons excite electrons from atom electron shells or give them enough energy to completely leave the atoms. In both cases, there is created a place with one missing electron. An electron from the upper energy level moves to the lower one and emits (characteristic) X-ray radiation. Kα is called the transition from L (the second energy level from nucleus, n=2) to K shell (the closest energy level to nucleus, n=1). The intensity of emitted characteristic X-ray radiation is much higher then the intensity of Bremmstrahlung radiation. Therefore, this source can be used even for XPS where we need source with one defined frequency ν.

The L shell has an inner subshells. L means that the principal quantum number is 2. We denote by K$\alpha_{1,2}$ the transitions $2p_{3/2} \rightarrow 1s$ and $2p_{1/2} \rightarrow 1s$. Energies of these transitions are too close to be distinguished. The energies of K$\alpha_{1,2}$ transitions are 1253.6 (0.70) eV for Mg and 1486.6 (0.85) eV for Al [15]. However, other transitions are also acceptable. Their intensity is lower but we can still see them in measured spectra as satellite peaks with lower intensity. The most significant is Kα_3 transition with relative intensity 9.2% for Mg and 7.8% fro Al anode. We can recognize the peaks emitted by their lines in our spectra by their relative intensity (with comparison to the peaks from K$\alpha_{1,2}$ doublet) and most importantly by their energy shift 8.4 eV (Mg anode) and 9.6 eV (Al anode) [15].

Completely different kind of X-ray source is a synchrotron. The synchrotron is a cyclic particle accelerator. Charged particles are accelerated by an electric field and a magnetic bending field holds them in stable trajectories. During the beam bending, particles loose their kinetic energy in a form of radiation. The direction of he emitted light is perpendicular to the beam movement direction. In suitable circumstances (kinetic energy, trajectory radius), there is emitted the continuous X-ray light with maximum at a critical frequency. The advantage is very high intensity of the emitted photons. On the other hand, the synchrotron is more complicated device than the X-ray tube and it is limited to bigger research groups.

The last step in XPS is the electron energy analyser. One of the most common analysers is an electrostatic hemispherical analyser (HSA). This type of analyser was also used during measurements for this thesis. The HSA consists of two concentric hemispheres with a gap between them. The hemisphere with the greater radius has a negative potential and the smaller one has a positive potential

with respect to passing electrons. Electrons enter the gap between hemispheres. They are repelled from the grater hemisphere and attracted to the smaller one. This electric field causes the electron beam to bend. The radii of electron paths depends on their initial kinetic energies. If their initial kinetic energy is too low or too high, electrons crash into one of the hemispheres. Only electrons with a small range of kinetic energies can pass through the analyser. We choose the detected kinetic energy of the electrons by changing the potential between hemispheres. The electrons which pass the analyser, i.e., with known kinetic energy, go to the detector that counts the amount of them for a chosen constant time.

2.2 RAIRS

Vibrational spectroscopies are complementary analysis methods to XPS. They are used for study and identification of chemicals in solid, liquid or gaseous samples. Vibrational spectroscopies are based on measurements of the frequencies which are absorbed by the sample. These frequencies correspond to vibrational modes in molecules which depend on chemical bonds between atoms and structures of particular molecules [16, 17, 18]. The range of energies related to vibrational modes is included in infrared region of the electromagnetic spectrum.

The total energy E_{tot} of a molecule is given by equation 2.2 [19] where E_{el}, E_{vib}, E_{rot} and E_{tra} represents electronic, vibrational, rotational and translational energies, respectively.

$$E_{tot} = E_{el} + E_{vib} + E_{rot} + E_{tra} \tag{2.2}$$

The electronic energy is an eigenvalue of molecular the Hamiltonian acquired by solving the Schrödinger equation. The rotational and the translational energies depend on the molecular movement. The vibrational energy is the one important for vibrational spectroscopies. It represents the energy of the vibrational movement of bonded atoms about their mean positions. The quantum theory gives us a discrete spectrum of possible energies for these vibrations. We can use a physical model of two bonded atoms and find eigenvalues of the corresponding Hamiltonian. However, the solution is not easy to be found. In order to simplify the equation, we commonly use the Born-Oppenheimer and the harmonic approximation. This model gives results good enough for the ground state. The discrete energy spectrum implies the existence of particular frequencies which are absorbed by the molecule and used for transition to a higher vibrational energy state. These resonant frequencies are affected by the bond strength and mass of atoms. Other physical models and detail description of an incident photon interaction with molecules can be found in work by Chabal [20].

The molecules, except for the simplest ones, can contain large number of atoms which means that many frequencies are equivalent to atom bonds. The number of possible vibrations, so called vibrational modes, depends directly on the number of atoms in the molecule. For linear molecules, the number of vibrational modes is determined by the equation 2.3. If the molecule is nonlinear, the number of modes is given by the equation 2.4 [19]. In the equations 2.3 and 2.4, n is the number of vibrational modes and N is the number of atoms forming a molecule.

$$n = 3N - 5 \tag{2.3}$$

$$n = 3N - 6 \tag{2.4}$$

For instance, water is a chemical substance with nonlinear molecules created by three atoms, two hydrogens and one oxygen. Under the equation 2.4, it has 3 vibrational modes depicted in Figure 2.1. There is a symmetrical stretching, an antisymmetrical stretching and a scissoring. Nevertheless, a water absorbance spectrum, which includes peaks corresponding to the vibrational modes, is more complex. It is due to the capability of hydrogen bond creation. Therefore, water molecules can bond to each other and this additional bond shifts the vibrational energies. That demonstrates the important effect related to all atom groups in molecules. If more different molecules contain the same atom groups, we can find the same peaks in acquired spectra although these peaks can be shifted. Hence, there are extensive databases of spectra which include reference measurements of different kinds of groups.

The vibrational spectroscopies are based on a detection of transmitted or reflected light. We focus only on reflection spectroscopies. Reflection absorption spectroscopies are limited by surface selection rules. Oscillating electric field excites only vibrational modes with the dipole moment perpendicular to the surface. Therefore, the number of modes which can be detected depends also on the angle of the incident light. Realizations of measurement instruments differ. The one used for data acquisitions in this thesis exploits the Fourier transform. Thus, it is sometimes called the Fourier transform reflection absorption spectroscopy (FT-RAIRS). The spectrometer itself consists of an infrared light source, an interferometer, a sample chamber and a signal detector. The infrared light source emits a beam of photons whose frequency range corresponds to the infrared region in the electromagnetic spectrum. The light from the source contains all frequencies we want to measure. A function of the next component, the interferometer, is to select a measured frequency. Due to the interferometer arrangement, it is called Michelson interferometer. It consists of a beam splitter and two mirrors. The beam splitter divides the light from the source into two beams. The angle included by the incident beam and the spliter surface tangent is 45°. That ensures the right angle between the reflected and the transmitted beam. Each beam is reflected from one of the mirrors and directed back to the splitter. The two beams are divided into four but we are interested only in the two of them which have the same direction. We could say that the splitter puts the beams together into one beam which goes to the sample compartment. In fact, the two beams interfere with each other. Whether their interference is constructive or destructive, that depends on the frequency of the beams and their retardation. The retardation is

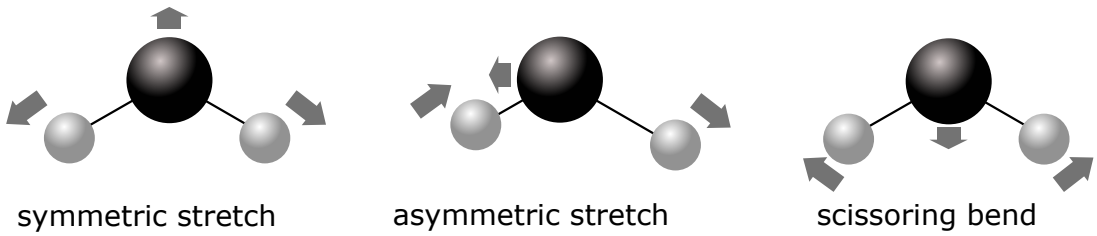

Figure 2.1: H_2O vibrational modes. Dark molecules represent oxygen and light ones represent hydrogen.

the difference between optical paths which the two beams travel. The only path which is not the same for the beams is from the splitter to the mirror, known as an arm of the interferometer, and back. Thus, the retardation is twice the difference between the lengths of the interferometer arms. By changing the retardation, we acquire an interferogram, i.e., the beam intensity dependence on the retardation. Changes in the retardation is achieved by fixing one mirror and moving the other one. We can obtain the intensity dependence on frequency by the Fourier transform application. Before the beam detection, we let it reflect off the surface where the vibrational frequencies are absorbed.

Each splitting procedure divides the beam intensity. Ideally 50% is reflected and 50% is transmitted. As a result, the ideal intensity of the beam heading for the sample is 50% relative to the original beam intensity from the light source. A great advantage of FT-RAIRS is that one measurement through all IR spectrum means moving of one mirror which takes only a few seconds.

2.3 TDS

Thermal desorption spectroscopy (TDS), also known as temperature-programmed desorption (TPD), is the method based on recording a partial pressure of desorbed molecules.

3. Experimental

3.1 Equipment

3.1.1 XPS apparatus

All XPS measurements are acquired under the UHV conditions in a vacuum chamber. The working pressure during the measurements was around 10^{-7} Pa. It was detected by an ion gauge. For achievement of a stable pressure level, a system of evacuation devices is used. The space in the vacuum apparatus is divided into two parts which are separated from each other by an airlock. When a new sample is considered to be put into the apparatus, the airlock is closed and the sample is inserted into the first part of the chamber. At that time, the part of the chamber with the sample contains an air at atmospheric pressure (1 atm). Nevertheless, the other part keeps its pressure steady (10^{-7} Pa). The initial evacuation of the first part containing the sample is ensured directly by a scroll pump. This type of a vacuum pump can achieve pressure in the order of pascals. Thereafter, a tubomolecular pump is added between the scroll pump and the chamber containing sample. This pump is designed to obtain high vacuum. Because it does not hold the pressure difference between HV and 1 atm it is pre-evacuated by the scroll pump. At this moment, the part of the chamber with sample has pressure at 10^{-5} Pa and the other one $10^{-7}Pa$. The airlock separating them can be opened and sample transferred to the chamber space with UHV. During this operation, the connection between two parts of chamber causes a pressure deterioration in the UHV section but the effect is just temporary. After the sample placement procedure is done, the airlock is closed and the conditions in UHV chamber are restored. The UHV chamber itself is evacuated by titanium sputter ion pumps. The apparatus is also equipped with titanium sublimation pump which is used only for a short time if a rapid pressure improvement is needed.

The UHV apparatus is a multifunctional device. Its schematic diagram is shown in Figure 3.1. It allows to perform XPS, termodesorption spectroscopy using quadrupole mass spectrometer (QMS), gas adsorptions, Ar^{+2} ion bombardments and depositions by micro-electron beam evaporation source (MEBES).

In the center of the vacuum chamber there is a specimen holder which contains six storage positions, so that six specimens can remain in a clean UHV environment at the same time. The holder is attached to a carousel that is connected to a manipulator. This holding system allows us to move with our specimen along one vertical and two horizontal axes, all perpendicular to each other. Along with that, we can rotate with the sample through an arbitrary angle around the vertical axis. Therefore, we can change the sample position to the desired one.

One of the holder positions is used for a sample temperature control. The holder is connected to a liquid nitrogen reservoir by copper wire which ensures an appropriate heat transfer. The holder is also in contact to a thermionic cathode. The heat is generated by the cathode filament current and by the electron emission current. The amount of extracted heat by the nitrogen reservoir cannot be regulated. Hence, we use the high voltage generating the emission current to

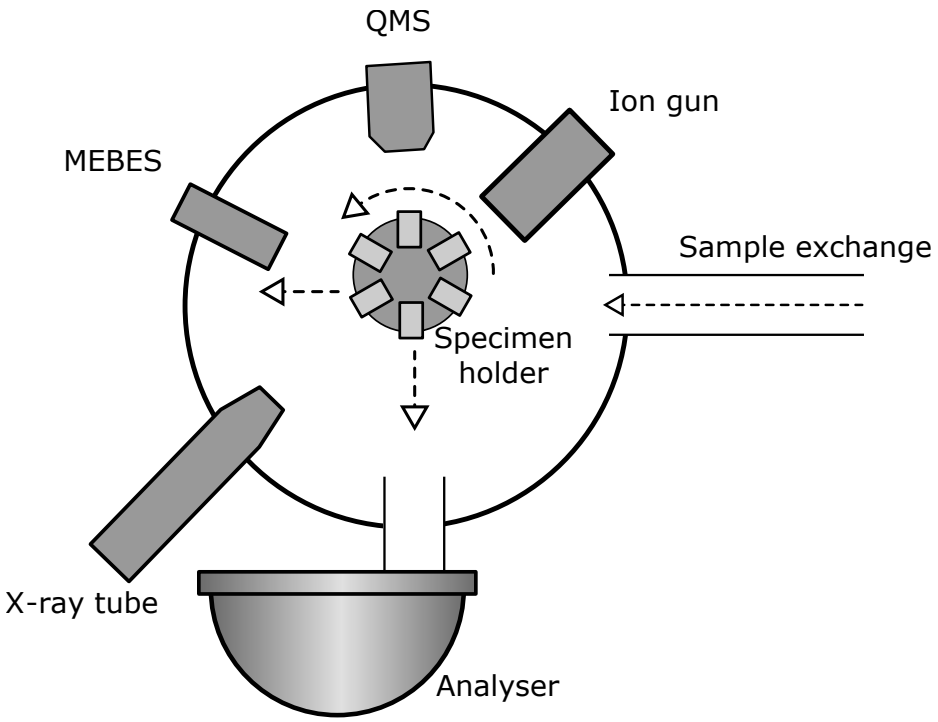

Figure 3.1: A schematic diagram of the UHV apparatus.

control the sample temperature. The operating electronic is configured to switch on/off the cathode high voltage in order to reach and maintain the preset temperature. A rate of the temperature increase is also optional. The temperature is obtained by a thermocouple attached to the holder. The thermocouple is closer to the heat source than the specimen. Thus, the sample temperature is less than the measured one. The difference between these values is approximately 15°C [21].

The XPS measurement system consists of an X-ray tube from VG and a hemispherical 5 channel analyzer Omicron EA 125. The X-ray source contains Al and Mg anode together. Before the measurement starts, we can switch between them to choose the more fitting one with respect to the experiment. The emitted electrons are accelerated by electric field 12 kV. The generated X-ray radiation pass through the output aperture which is closed by a thin aluminum foil. The thin Al foil demodelates an electric field around an anode and prevents from the pressure deterioration after the X-ray tube activation. Because of increased temperature, the atoms and molecules at the surface of inner parts of the tube desorb into the vacuum. Moreover, the aluminum layer helps to decrease the radiation intensity which belongs to photons with different frequencies than the frequency of a dominant characteristic X-ray radiation peak. The entire X-ray tube is movable and can be pushed at about 1 cm closer towards the sample. The sample position is set thus the surface plane is perpendicular to the direction of an analyzer input aperture.

The analyzer starts with an optical system which defines the measured area at the surface of a sample. This system of lenses and apertures focuses electrons to an entrance that leads to the space between the two analyser hemispheres. The inner hemisphere has a positive potential and the outer one a negative potential.

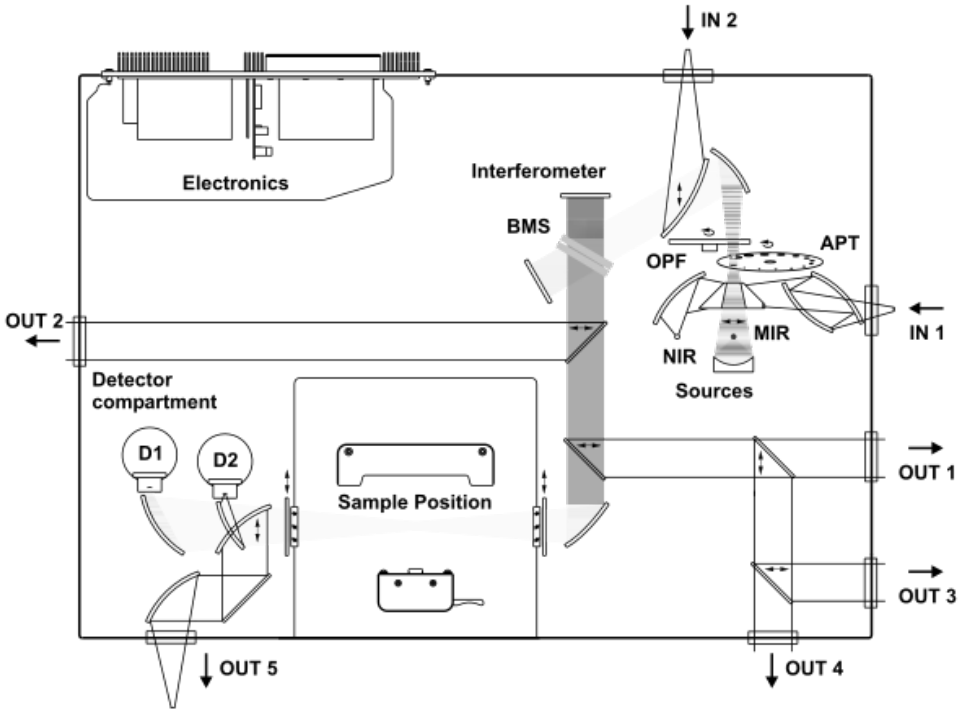

Figure 3.2: A schematic diagram of the FT-RAIRS apparatus VERTEX 70v [22].

The electrons are collected by a multichannel detector.

The apparatus is equipped with quadrupole mass spectrometer Leybold Inficon 2000.

3.1.2 RAIRS apparatus

The Fourier transform infrared instrument is a commercial device VERTEX 70v made by Brucker Corporation. Its schematic diagram is shown in Figure 3.2. Further information is included in [22]. The VERTEX 70v contains a MIR source, a silicon carbide, which emits infrared light. The interferometer consists of KBr beamsplitter that has a working range including IR light from 8000 to 350 cm^{-1}. The interferometer is followed by a sample compartment and a detector compartment. The detection is provided by a DigiTect DLaTGS detector with a spectral range from 12 000 to 250 cm^{-1}. There is a optical system of mirrors and lenses in order to create a suitable optical path connecting all spectrometer components. The spectrometer is evacuated by a scroll pump except for the sample compartment. Because the sample compartment is opened frequently, its space is separated from the rest of the apparatus and it has its own evacuation system. It is created by a turbomolecular pump which is connected to the scroll pump. There is an option to add a covering shield over the sample; or to decrease the space with improved vacuum guaranteed by the turbomolecular pump. That is useful for some specific applications, e.g. adsorptions and desorptions.

3.2 Specimen Preparation

The TiNb base material was prepared at The Czech academy of Science by the procedure described in [12]. The TiNb alloy were created by a method called arc-melting. This technique produces ingots with elevated homogeneity. The TiNb alloy consists of 74 % Ti and 26 % Nb. There were used a titanium ingot of high purity (containing 99.55 % of Ti) from Frankstahl (Austria) and a niobium ingot of high purity (containing 99.85 % of Nb) from TIC (Belgium). Firstly, the both ingots are melted by vacuum induction melting in a required ratio and form a new cylindrical object which is used as one electrode. The other electrode is created of the same alloy at the bottom of a crucible. The arc-melting process lies in enclosing the cylindrical electrodes to each other till an electric arc appears. There is a direct current of 800-1000 A between the electrodes which creates enough heat to remelt the cylindrical ingot. The whole procedure is executed in a vacuum in the order of pascals. The arc-melting process was repeated eight times. This was followed by solution annealing at 850°C for 30 min and quenching in water. A high homogeneous ingot was sliced by SiC cutting wheel. The sliced peaces with diameter of 10.5 mm and thickness of approximately 1.5 mm were proceed to a polishing.

The specimens were polished by sandpapers with different grit sizes. The sandpaper is a paper coated with an abrasive material. In order to make the surface smoother, several kinds of sandpapers were used. The sandpapers are distinguished by the size of particles selected as the abrasive material. There are established more standards of grid size designation. All of them are referred to the average grit size. One of the most common is the United States system called the CAMI (Coated Abrasive Manufacturers Institute). The sample surface was polished sequentially by 240, 600, 800, 1000 and 4000 grit. The specimens preparation described up to this point was performed by coworkers from The Czech academy of Science.

The following procedures were made at Department of Surface and Plasma Science, Faculty of Mathematics and Physics, Charles University in Prague. The diamond paste with abrasive powder was subsequently used. Its designation is D 20, D 7, D 2 and D 0.2 which corresponds to the average grit size of 20, 7, 2 and less than 1 μm.

Polished samples were cleaned by an ultrasonic bath. The ultrasonic cleaning is an effective process of removing contaminants attached to the surface. Ultrasonic sound waves travel through the liquid causing rapid changes of pressure. That leads to the creation of cavitation bubbles. They are small void space bubbles which implode. The implosion generates an intensive shockwave. Samples were cleaned by using an ethanol solution. Samples immersed in the solution were exposed to the cavitation for 5 minutes.

3.3 Experiment Description

All of the TiNb specimens underwent the polishing procedure and the ultrasonic cleaning. A total amount of six samples was divided into two groups. The first one was naturally oxidized in the open air. This process occurs spontaneously. During the polishing, oxidized layers are removed from the sample surface and

pure metal parts are uncovered. The titanium and the niobium are extremely reactive elements. Therefore, it causes the immediate oxidation after they get in contact with the oxygen in the air. However, this process is so fast that a few passivative layers of thickness several nanometers of a stable oxidized titanium and niobium protect the deeper layers. The other half of specimens was oxidized thermally. The samples were heated in the furnace surrounded by air with a step of 10°C per minute up to 600°C and this temperature was held for 1 hour. They were kept in the furnace till it cooled to the temperature about 200°C and then they were let to cool to the room temperature outside the furnace.

Two specimens treatments were performed. Firstly, the water treatment procedure of two samples, a natural oxide and a thermal oxide, is described. After the preparation procedure, the naturally oxidized specimen was inserted into the UHV apparatus and an XPS spectra was acquired. All following XPS measurements (this one included) consists of a spectrum of a wide scan and more precise spectra of a valence band and peaks of Ti 2p, Nb 3d,O 1s and C 1s and Ti Auger electrons. The wide scan consists of 1 measurement through energy range from 0 to 1000 or 1100 eV. Contrary to the wide scan, the other spectra were created by the combination of data from several scans over a chosen range (usually around 10 scans). After the XPS procedure, the sample was taken out and soaked in H_2O heated at 100°C for 1 h. An XPS of the H_2O treated natural oxide was measured in UHV. The sample was kept still in UHV while the thermodesorption spectroscopy was performed. During the TDS procedure, sample was heated up to 400°C with heating rate of 2°C/min and the temperature was hold at 400°for 5 min. In all following TDS, the rate and the time are the same, unless otherwise stated. After the sample cooled down to the room temperature, an XPS spectra were taken.

The other specimen treated by H_2O is the thermally created oxide. It underwent the same procedure as the natural oxide. It means that the XPS spectra was acquired after the thermal preparation. Afterwards, it was boiled in 100°C water for 1 h and measured by XPS. TDS (400°C) was performed followed by the XPS.

Secondly, two samples, a natural and a thermal oxide, were treated by 5M NaOH. The 5M NaOH was prepared by combining 20 g of granulated NaOH and deionized water of total volume (including NaOH) 100 ml. This endothermic reaction heats the NaOH water solution at 60 °C. That temperature was hold for the entire time of the sample immersion by an external heat source. Compared to the H_2O XPS measurements, a range of binding energies Na 1s is added.

The naturally oxidized specimen was inserted into the UHV apparatus and an XPS spectra were acquired. Subsequently, it was soaked in 5M NaOH at 60°C for 5 min. Afterwards, an XPS was acquired followed by the TDS (400°C, 5 min).

The thermally oxidized sample was treated by 5M NaOH at 60°C for 10 min. Thereafter, the XPS was measured. There was a TDS (400°C, 5 min) performed and consequently an XPS spectra acquired.

Two of the samples were used for the RAIRS. The first specimen was a natural oxide and the other one was a thermal oxide. After the RAIRS, the second one was treated by NaOH and measured by the RAIRS again.

The natural oxide was inserted into the RAIRS apparatus and measured. Afterwards, it was heated up to approximately 360°C and kept at that temperature

for 5 min. The specimen was cooled down to the room temperature and measured by the RAIRS.

The thermal oxide was measured *as received* by the RAIRS. After that, it was soaked in 5M NaOH at 60°C for 10 min. The RAIRS was consequently performed. This data acquisition was followed by heating up to 360°C for 5 min (at that temperature). After the sample cooled down to the room temperature, a RAIRS spectrum was measured.

4. Results and Discussion

4.1 XPS Measurements

4.1.1 Peak Assignment

A position of the Nb $3d_{5/2}$ peak at 207.2 eV corresponding to Nb_2O_5 [23] is used as a reference energy for the binding energy calibration of acquired spectra as shown in Figure 4.1. One of the measured samples (natural oxide treated with H_2O after TDS) is in a reduced state. Thus, it does not contain the Nb_2O_5 peak. The energy shift is caused by a material charging. Insulating materials, e.g., oxides, cannot refill emitted electrons fast enough and a local charge is created at the surface. In case of conductors, the charge shift should be none or very small. Therefore, the spectrum without the Nb_2O_5 peak is calibrated by checking the binding energies of metal Nb $3d_{5/2}$ at 202.1 eV and the O 1s peak at 530.5 eV (bonded with Ti and Nb) [23], in Figure 4.2. The O 1s dominant peak position corresponds to the positions in the rest of the spectra.

For a processing of all spectra, the Shirley background subtraction and the Voigt form of peaks were used. All spectra are normalized to maximum so that we could better see the relative changes in peak intensities. Nevertheless, the overall areas of the spectra can be directly determined from the table comparing surface element compositions (Table 4.1).

Ti 2p lines of all measurements are depicted in Figure 4.3. Voigt peaks with the full width in a half maximum (FWHM) ≈1.5 eV are used for data fittings. In Figure 4.3, doublets of Ti $2p_{1/2}$ and $2p_{3/2}$ are observed. In Figure 4.3, only the peaks with lower energies (Ti $2p_{3/2}$) are designated. A majority of the spectra contains only the peak denoted by Ti(1). Ti(1), at the binding energy of 458.8-459.0 eV, was assigned to TiO_2. The separation Δ between Ti $2p_{3/2}$ and the $2p_{1/2}$ (higher energy) is for Ti(1) 5.72 eV. The position of the TiO_2 line and the separation corresponds to the literature values [23, 24, 25]. Ti(2) with binding energy at 457.6 eV is attributed to Ti_2O_3 [24, 25, 26]. Due to the low intensity of the Ti_2O_3 $2p_{3/2}$ line, the $2p_{1/2}$ line with lower intensity was not fitted. The Ti line shape requires the peak Ti(3), at 456.3 eV and with Δ 5.70 eV. However, its origin is not clarified. No corresponding titanium bond at that energy was found. Ti(3) could be a result of imperfect fitting procedure, e.g., background subtraction, peak shape. Ti(4) and Ti(5) lines has binding energies at 454.9 and 454.0 eV with separations Δ 5.72 and 6.17 eV, respectively. The former one is attributed to TiO and TiC (titanium carbide, can be determined from C 1s spectrum) and the latter one to metallic Ti [27, 28, 29, 23, 25]. Kα_3 were taken into account. It creates a duplicate of the measured K$\alpha_{1,2}$ peak with 8% of original intensity and a shift of 8.4 eV to the lower binding energy. This satellite peak was created only for the Ti $2p_{1/2}$ peaks with the highest intensity because they appear near the Ti $2p_{3/2}$ peaks and could effect the result fit.

Figure 4.1 includes all measured spectra of Nb 3d line. The spectra consist of Nb $3d_{3/2}$ and $3d_{5/2}$ doublets. Except for one, all spectra could be fitted by one doublet Nb(1) with binding energy Nb $3d_{5/2}$ at 207.2 eV and separation $\Delta = 5.76$ eV. This peak was used as a reference for the spectra calibration and is

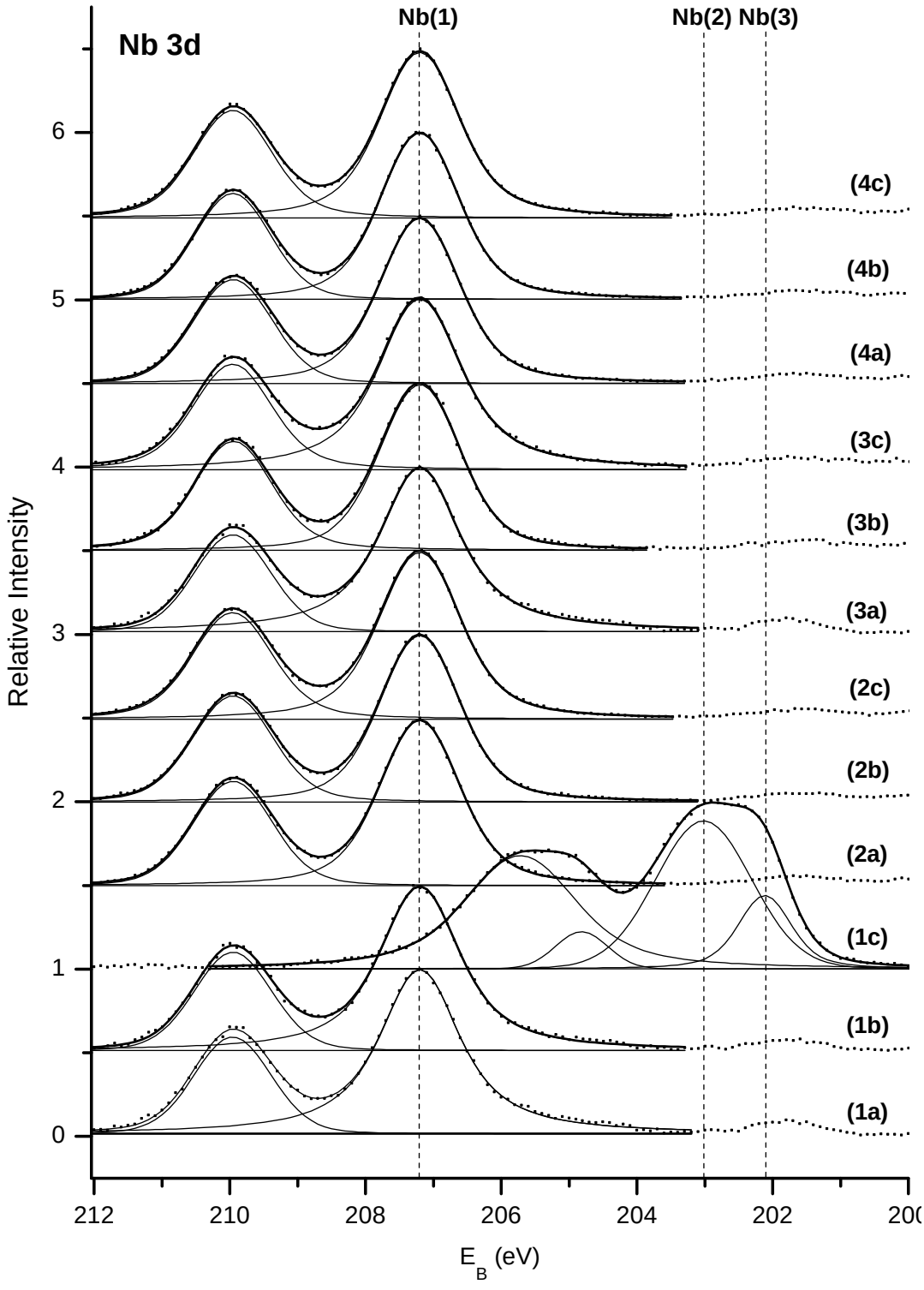

Figure 4.1: Nb 3d spectra of the natural TiNb oxide treated with H_2O (1a, 1b, 1c), the thermal one treated with H_2O (2a, 2b, 2c), the natural one treated with NaOH (3a, 3b, 3c) and the thermal one treated with NaOH (4a, 4b, 4c). The letters in brackets describe spectra before and after the treatment and after the TDS, respectively.

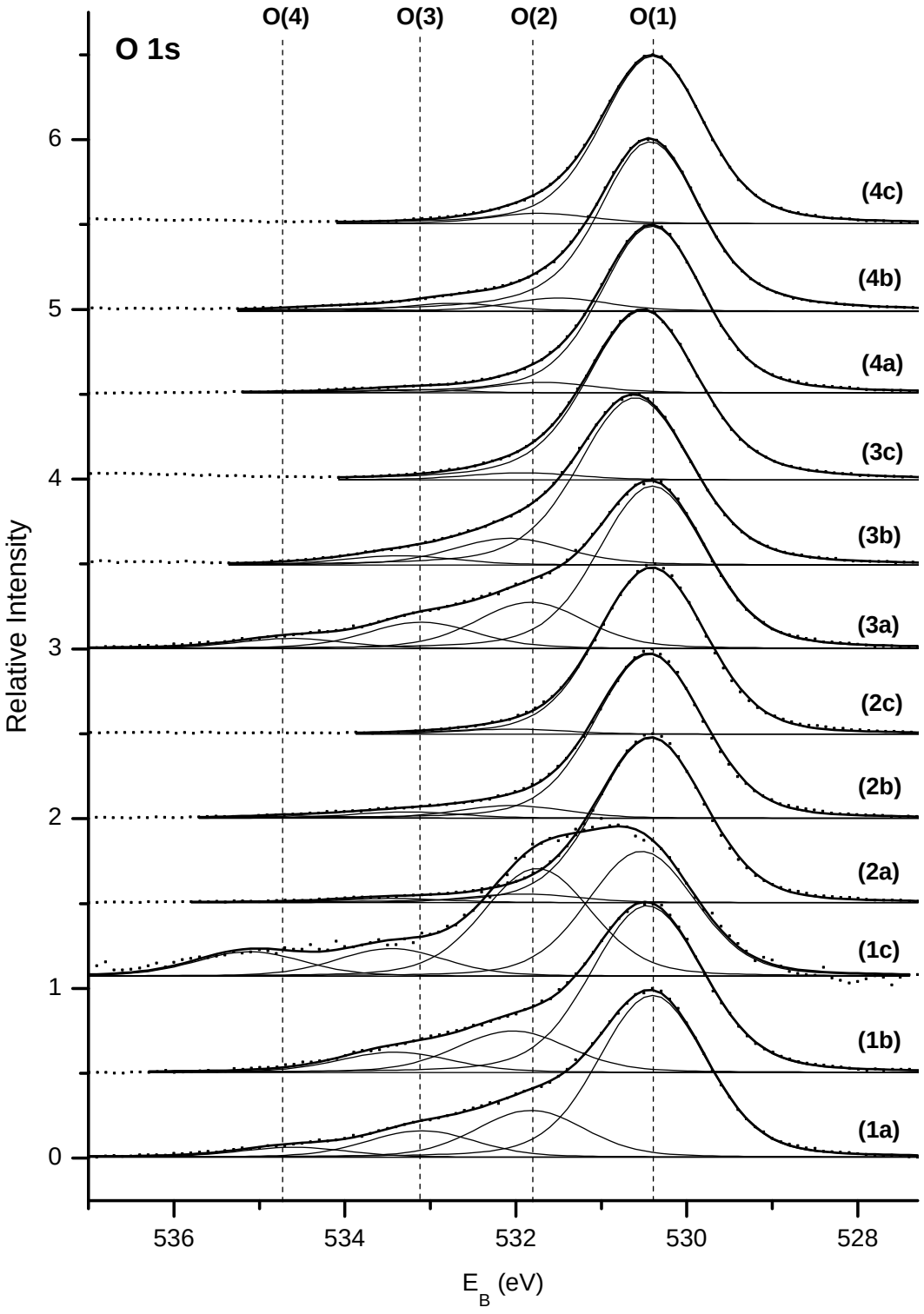

Figure 4.2: O 1s spectra of the natural TiNb oxide treated with H_2O (1a, 1b, 1c), the thermal one treated with H_2O (2a, 2b, 2c), the natural one treated with NaOH (3a, 3b, 3c) and the thermal one treated with NaOH (4a, 4b, 4c). The letters in brackets describe spectra before and after the treatment and after the TDS, respectively.

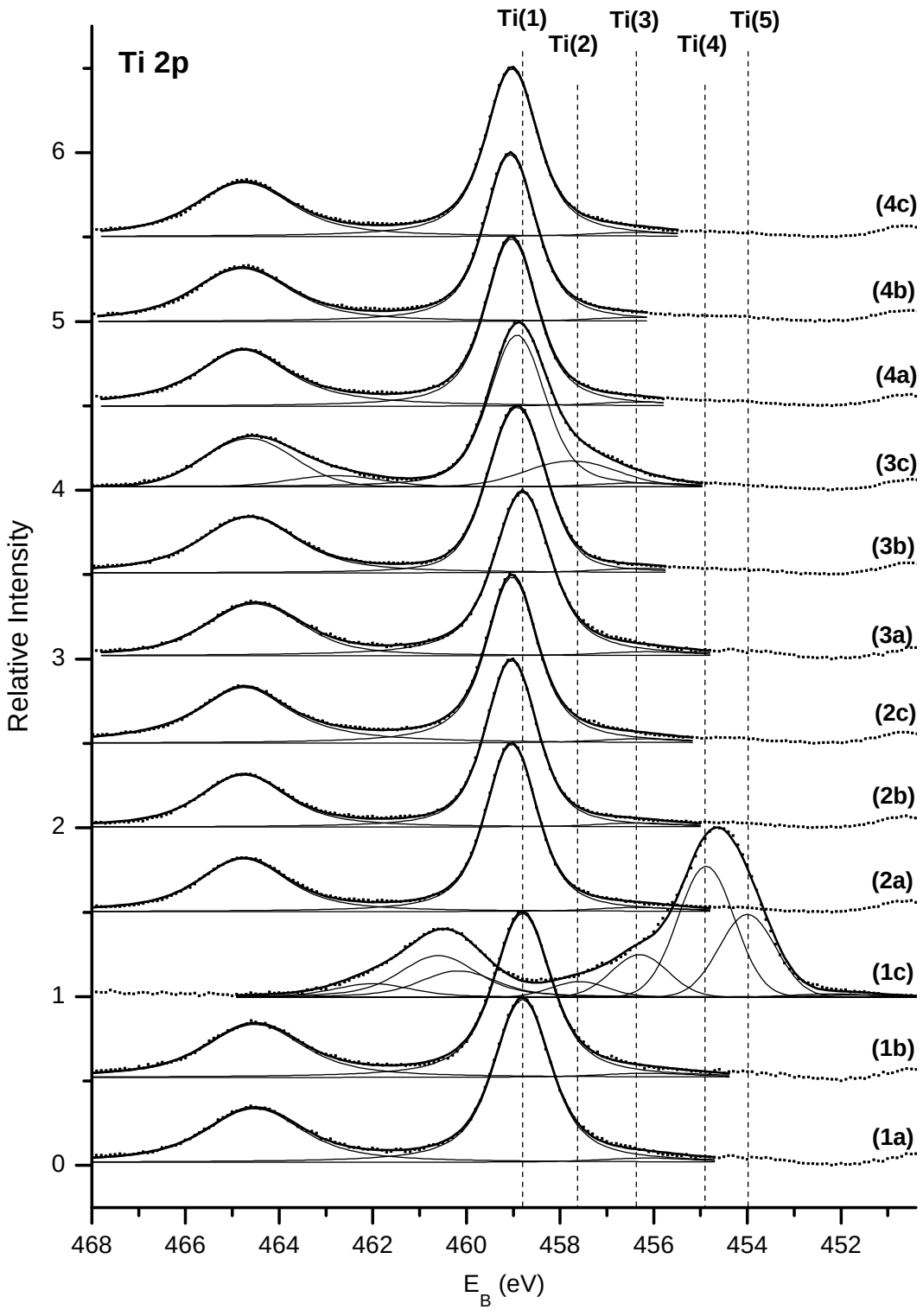

Figure 4.3: Ti 2p spectra of the natural TiNb oxide treated with H_2O (1a, 1b, 1c), the thermal one treated with H_2O (2a, 2b, 2c), the natural one treated with NaOH (3a, 3b, 3c) and the thermal one treated with NaOH (4a, 4b, 4c). The letters in brackets describe spectra before and after the treatment and after the TDS, respectively.

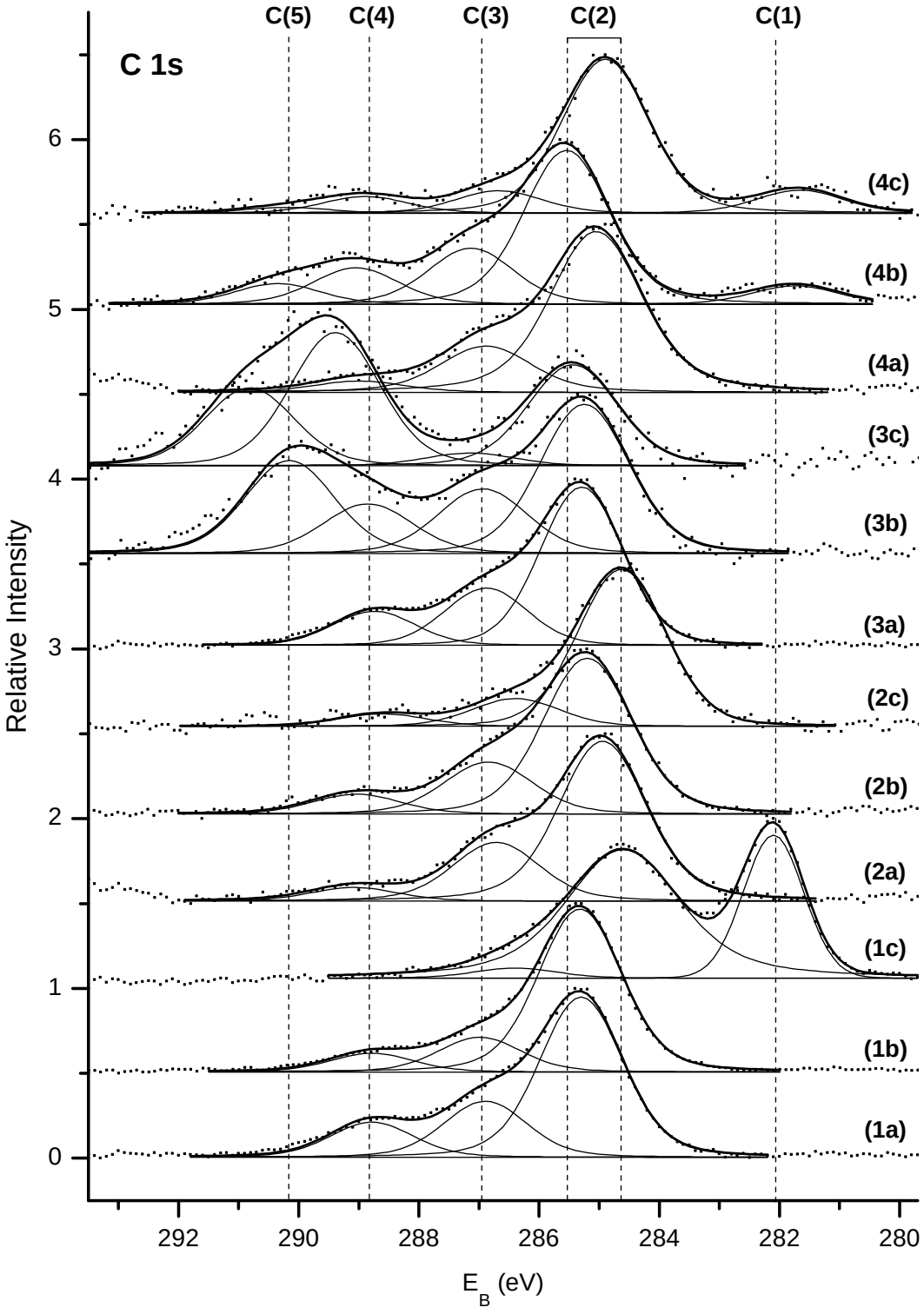

Figure 4.4: C 1s spectra of the natural TiNb oxide treated with H_2O (1a, 1b, 1c), the thermal one treated with H_2O (2a, 2b, 2c), the natural one treated with NaOH (3a, 3b, 3c) and the thermal one treated with NaOH (4a, 4b, 4c). The letters in brackets describe spectra before and after the treatment and after the TDS, respectively.

Table 4.1: The percentage elemental composition of TiNb surface of naturally oxidized samples and thermal oxidized samples immersed in H_2O or NaOH. There are three measurements for each sample and treatment, before and after treatment and after termodesorption (TDS).

	H_2O natural			H_2O thermal			NaOH natural			NaOH thermal		
	before [%]	after [%]	TDS [%]	before [%]	after [%]	TDS [%]	before [%]	after [%]	TDS [%]	before [%]	after [%]	TDS [%]
Ti	12	10	25	17	15	19	12	18	18	18	17	20
Nb	5	4	12	8	7	8	5	3	4	8	6	7
O	53	43	15	62	59	64	55	62	68	61	63	66
C	30	43	48	13	19	9	28	17	10	13	14	7

attributed to Nb_2O_5. The one different spectrum consists of two peaks Nb(2) and Nb(3) at 203.0 and 202.1 eV with separations Δ of 2.70 eV (both), respectively. The former peak is attributed to NbO and the latter one to metallic Nb. These results correspond to the literature [23]. Between energies Nb(2) and Nb(3) is the binding energy of carbidic bond NbC, 202.5 eV [30]. This is further discussed in section 4.1.2.

C 1s core level region is shown in Figure 4.4. Five different peaks were found. The first one, designated by C(1), is at position from 281.7 to 282.1 eV and is related to the carbidic carbon (TiC, NbC) [27, 28, 29, 30]. The position of second one, C(2), is from 284.6 to 286.6 eV. This range of energies is related to the summary of different kinds of carboneus contamination. It includes graphite (C-C) and aliphatic hydrocarbons (C-H) [31, 12, 32]. The third peak C(3), at 286.4-287.2 eV, is attributed to the C-OH and ether (C-O) groups [31, 24, 33]. C(4) has position at binding energy from 288.8-289.4 eV. The maximal value for the range is given by the spectrum of a natural oxide treated in NaOH after a thermodesorption, Figure 4.4 (3c). This spectrum has low intensity which means that the fit is less accurate. Except for this spectrum, the other ones containing this peak (10 spectra out of 12) have their positions in the range 288.8-289.0 eV. This energy range of C(4) is assigned to the carbonyl groups (C=O) [31, 24, 33]. The fitted peak C(5) is at position from 290.2 to 290.8 eV. As in case of C(4), the range without spectrum (3c) in Figure 4.4 is from 290.2 to 290.4 eV. This energy of C 1s line denoted by C(5) is attributed to the various carboneus species, e.g., carbon with more than one oxygen.

O 1s lines for measured samples are depicted in Figure 4.2. Voight peaks with FWHM equal $\approx$1.5 eV are used for O 1s curve fittings. The number of used peaks is 4. We denote by O(1) the peak at binding energy 530.4-530.6 eV. It is related to the Ti and Nb oxides [25, 24, 2]. O(2), at position 531.5-532.0 eV, is assigned to OH^- and carbonyl (O=C) groups [31, 32, 24, 7, 34, 26]. O(3) peak is at energy from 533.5 to 533.1 eV and is attributed to the ether groups (C-O) and chemisorbed water [31, 32, 24, 34, 26]. The position of peak designated by O(4) is 534.6-535.1 eV. It has low intensity and due to the higher binding energy, the origin of this peak is ambiguous. This peak might by associated with carboneous contamination, e.g., C-O-C bonds.

The relative surface elemental composition of measured samples was evaluated by using relative sensitivity factors. Calculated percentage values are shown in

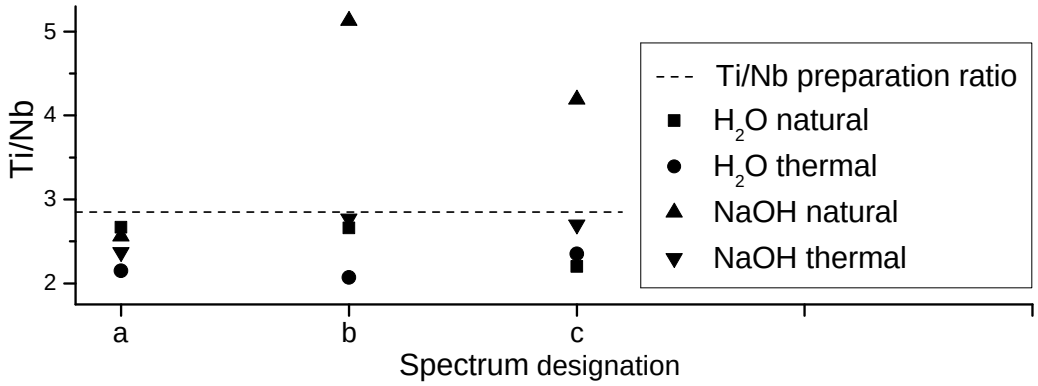

Figure 4.5: Ti/Nb ratio of the natural TiNb oxide treated with H_2O, the thermal one treated with H_2O, the natural one treated with NaOH and the thermal one treated with NaOH. The letters a, b and c describe spectra before and after the treatment and after the TDS, respectively. The dashed line shows the Ti/Nb ratio of melted elements during the TiNb alloy preparation.

Table 4.1. After NaOH treatment, the Na 1s peak was observed (not shown in this work). It creates less than 1% of all present elements at the surface.

The percentage values of Ti and Nb from Table 4.1 were used to create the Ti/Nb ratio. The data are depicted in Figure 4.5. In Figure 4.5, there is also shown the manufactured Ti/Nb ratio, 74%/26%.

The significant change in the Ti/Nb concentration is between spectra of natural TiNb oxide treated with NaOH denoted by (3a), (3b) and (3c). Before the treatment (3a), the Ti/Nb ratio corresponds to the ratios of other samples. After the treatment (3b), the amount of Ti presented at the surface is significantly increased. Following TDS (3c) partially returns the ratio to its expected value. The similar effect might be seen on a smaller scale in case of thermal oxide treated with NaOH (4a, 4b, 4c). However, the changes of the thermal oxide ratio are, with respect to deviations, too small in order to determine whether the same effect is present or not. More data are required so that a general conclusion about NaOH treatment could be created. Except for the two spectra of natural oxide soaked in NaOH (3b, 3c), the rest ten values of Ti/Nb ratio are lower than the preparation one represented by the dashed line in Figure 4.5, i.e., there is more Nb at the surface than is expected. These results correspond to the project made in 2014 (Zdeněk Rafaj, Jakub Schusser. Study of biocompatible materials by methods of surface physics, KFPP MFF UK). The same alloy were used for *in situ* UHV experiments. There was also measured slightly greater concentration of Nb at the surface with respect to the expected value.

4.1.2 H_2O treatment of a natural oxide

Figures 4.6, 4.7, 4.8 and 4.9 show spectra of Ti 2p, Nb 3d, C 1s and O 1s, respectively. The relative intensities of depicted lines are normalized to their maxima. In each figure, there are three spectra measured before and after H_2O treatment and after TDS.

The Ti and Nb are after polishing in highly oxidized state TiO_2 and Nb_2O_5 which is determined from presence of Ti(1) and Nb(1) peaks in Figures 4.6 and

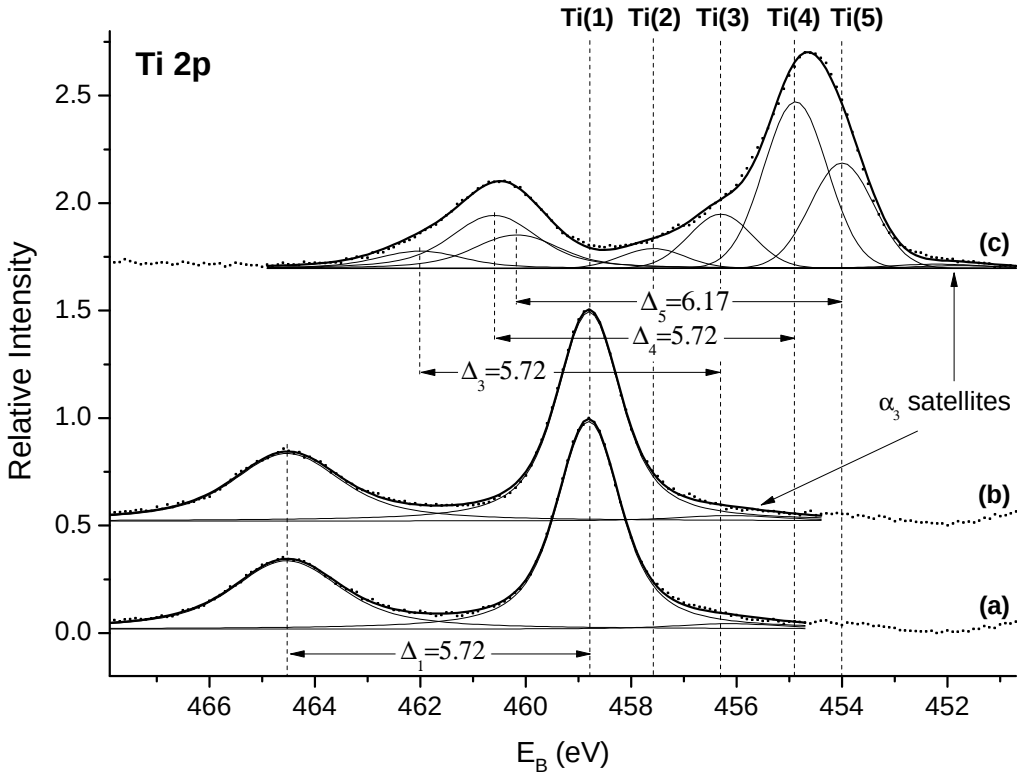

Figure 4.6: Ti 2p spectra of the natural TiNb oxide before (a) and after H_2O treatment (b) and after TDS (c).

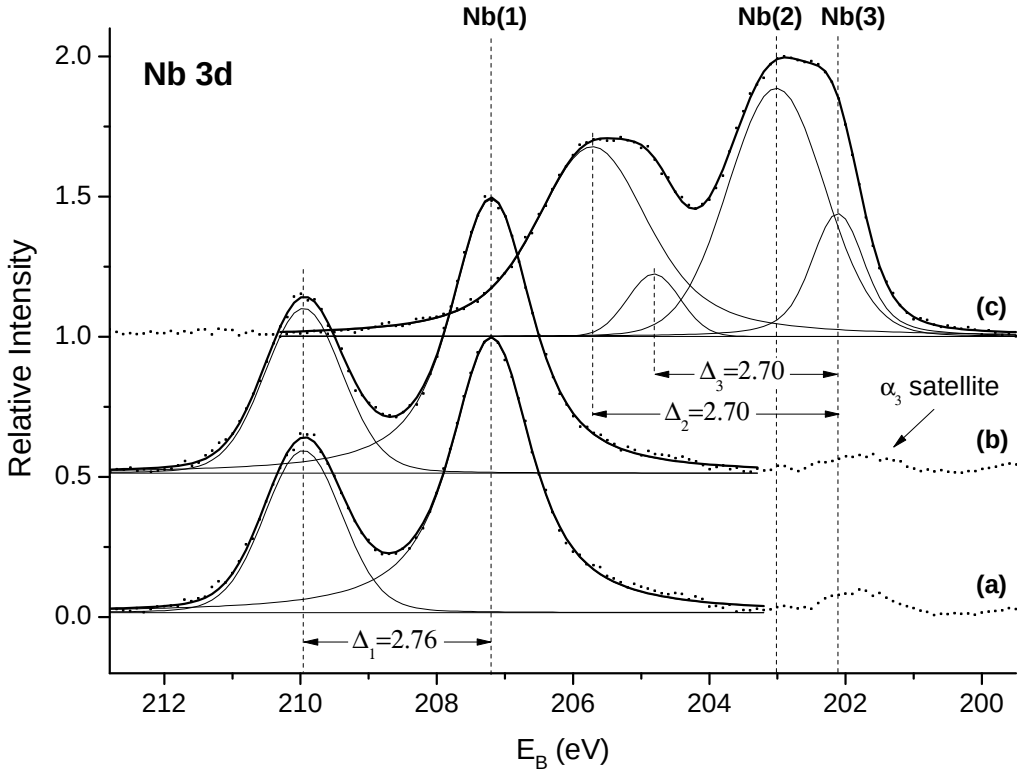

Figure 4.7: Nb 3d spectra of the natural TiNb oxide before (a) and after H_2O treatment (b) and after TDS (c).

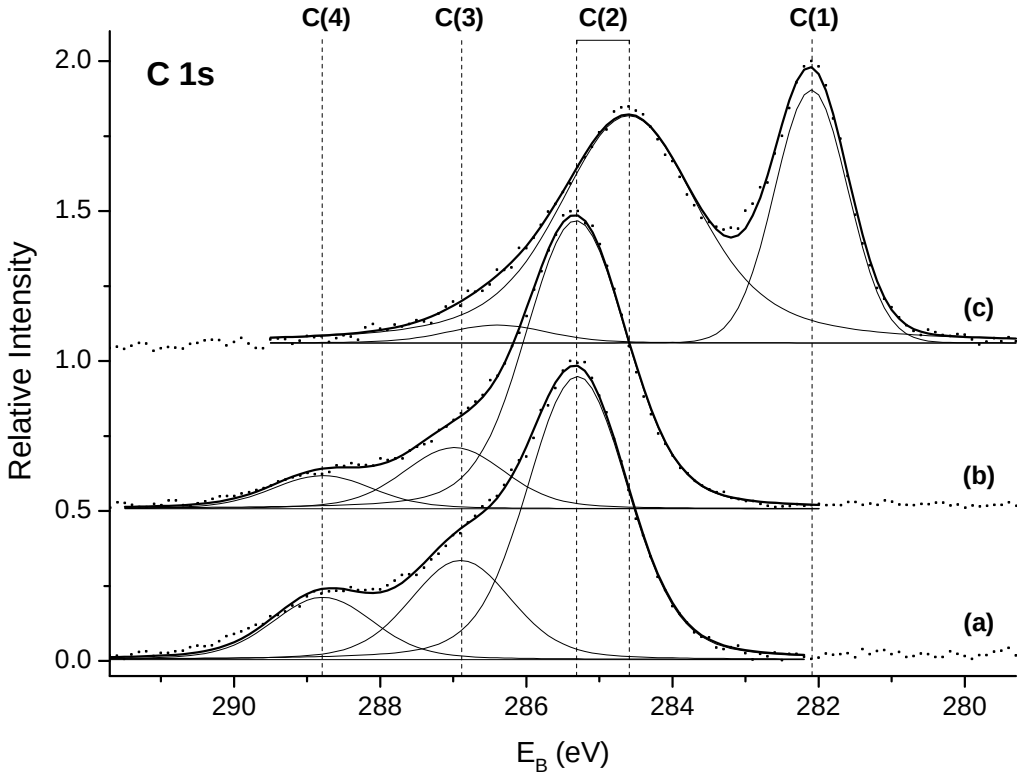

Figure 4.8: C 1s spectra of the natural TiNb oxide before (a) and after H_2O treatment (b) and after TDS (c).

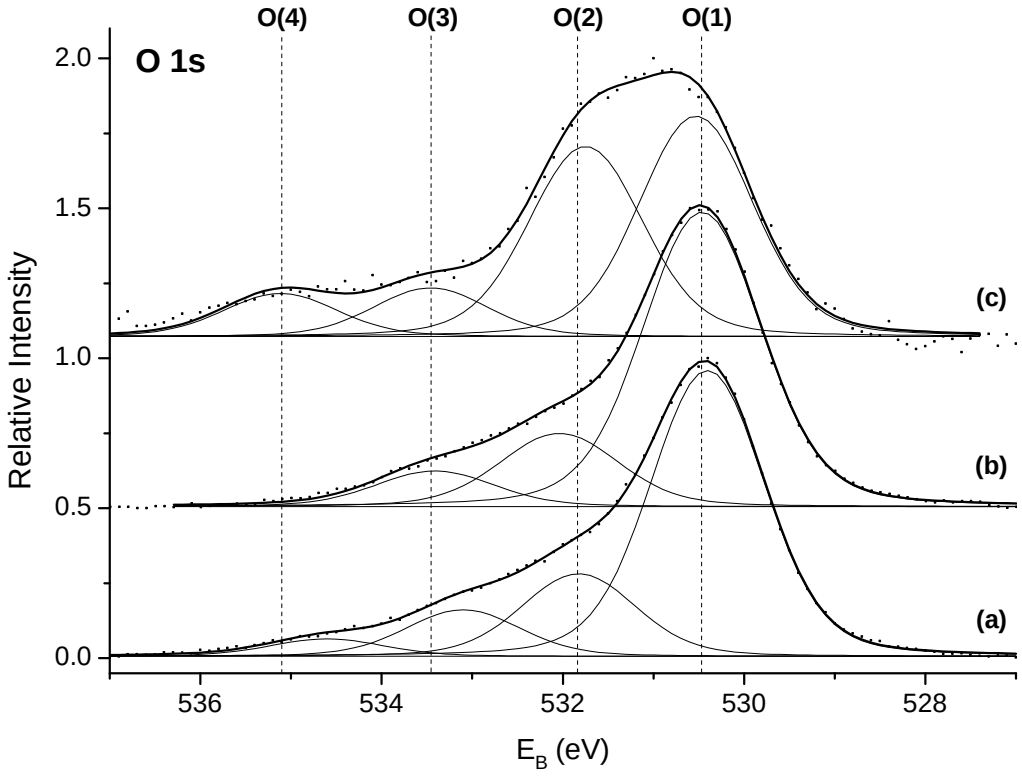

Figure 4.9: O 1s spectra of the natural TiNb oxide before (a) and after H_2O treatment (b) and after TDS (c).

4.7. After the H_2O boiling, no changes in Ti and Nb spectra are seen. After TDS, the titanium and niobium atoms are in significantly reduced states. Oxidized forms TiO_2 and Nb_2O_5 completely disappear and are replaced by lower oxides and metallic Nb and Ti. Nb(2) is attributed to NbO, Nb(3) to metallic Nb, Ti(2) to Ti_2O_3, Ti(4) to TiO and Ti(5) to metallic Ti. In Figure 4.6, there is also doublet denoted by Ti(3). Its binding energy was not assigned. No corresponding bond whose presence could be reasonably justified was found at that energy. Its origin might be connected with an imperfection of the fitting procedure, e.g., peak idealization. The ratio between Ti and Nb, in Figure 4.5, is a bit lower than the one expected from the preparation. Due to the deviations in XPS quantification, the ratio could be considered identical.

After the polishing procedure (a), there is 30% of C at the surface, see Table 4.1. It is mostly created by graphite and aliphatic carboneous species denoted by C(2). In Figure 4.8, the peaks C(3) and C (4) attributed to C-O and C=O are observed. After the H_2O treatment, the intensities of the C(3) and C(4) peaks are almost the same. However, the intensity of C(2) graphite peak grows (spectra without normalized intensity are not shown here). The overall surface concentration of C increases to 43%. After the sample heating, peaks C(2) and C(3) are significantly reduced, and C(4) completely vanishes while the carbide peak (Ti-C, Nb-C) designated by C(1) appears.

The O 1s lines consist of four peaks. They are depicted in Figure 4.9. The first one O(1) assigned to the Ti and Nb oxide (TiO_2 and Nb_2O_5) is after H_2O immersion without changes. Intensities of the O(2) and O(3) are slightly decreased and the O(4) peak completely vanishes. After the TDS, Ti and Nb are reduced which corresponds to the significant decrease in O(1) intensity. O(2) and O(3) are also decreased. Contrary to that, O(4) appears. OH groups bonded at TiNb surface are connected with the O(2) peak which also includes OH groups bonded to carbon and C=O groups. Considering the high concentration of carbon contamination on samples before and after treatment, the presence of OH groups bonded to the TiNb surface cannot be determined. After TDS, the most carboneous contamination is in a from of graphite and carbide. The overall concentration of O 1s is 15%. Thus, it is below the resolution of XPS quantitative analysis to calculate the amount of OH groups at the surface after this procedure.

Due to the significant changes in oxidation states of Ti and Nb, this experiment was independently repeated with another specimen with the same result.

4.1.3 H_2O treatment of a thermal oxide

It is presumed that Ti and Nb create thick layer of oxide. That confirms spectra in Figure 4.3 and 4.1 (2a, 2b, 2c). The thermally oxidized surface seems to be stable without changes in oxidation state or intensity during procedures. Ti and Nb create solely TiO_2 and Nb_2O_5. The Ti/Nb ratio is constant with respect to the deviations as shown in Figure 4.5.

Figures 4.10 and 4.11 show spectra C 1s and O 1s during the H_2O treatment of the thermally oxidized sample. The vertical axis shows the relative intensities of lines normalized to their maxima. Each figure contains three lines corresponding to the measurement before and after H_2O treatment and after TDS.

After the thermal oxidation, there is 13% of carbonous contamination at the

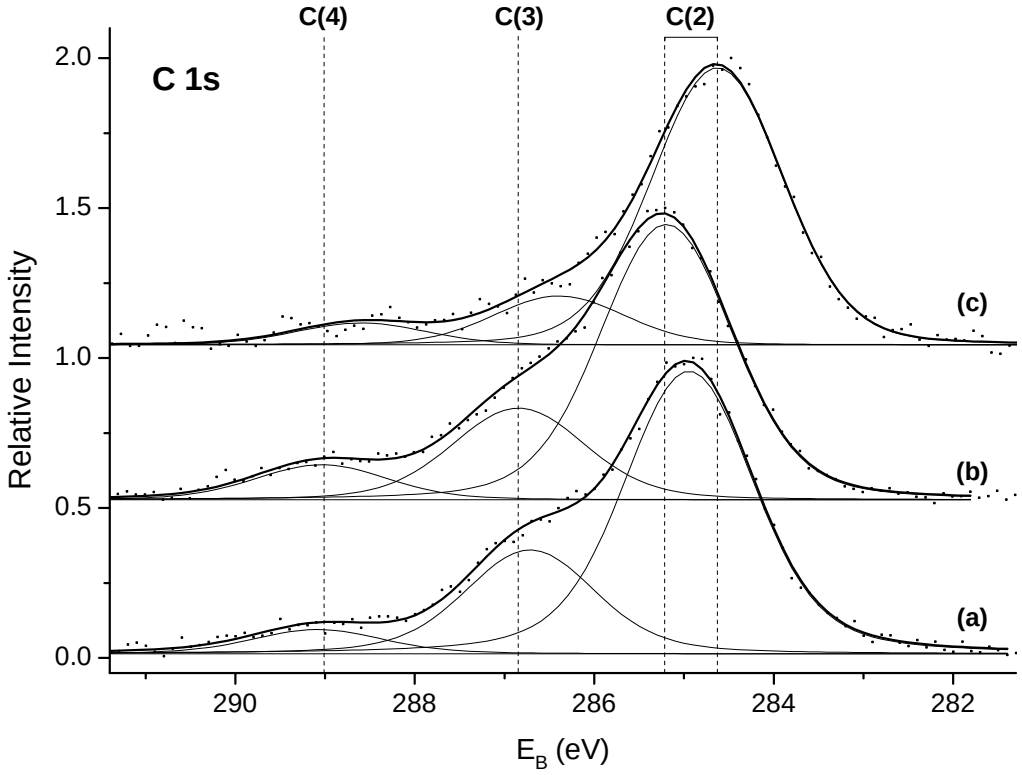

Figure 4.10: C 1s spectra of the thermal TiNb oxide before (a) and after H_2O treatment (b) and after TDS (c).

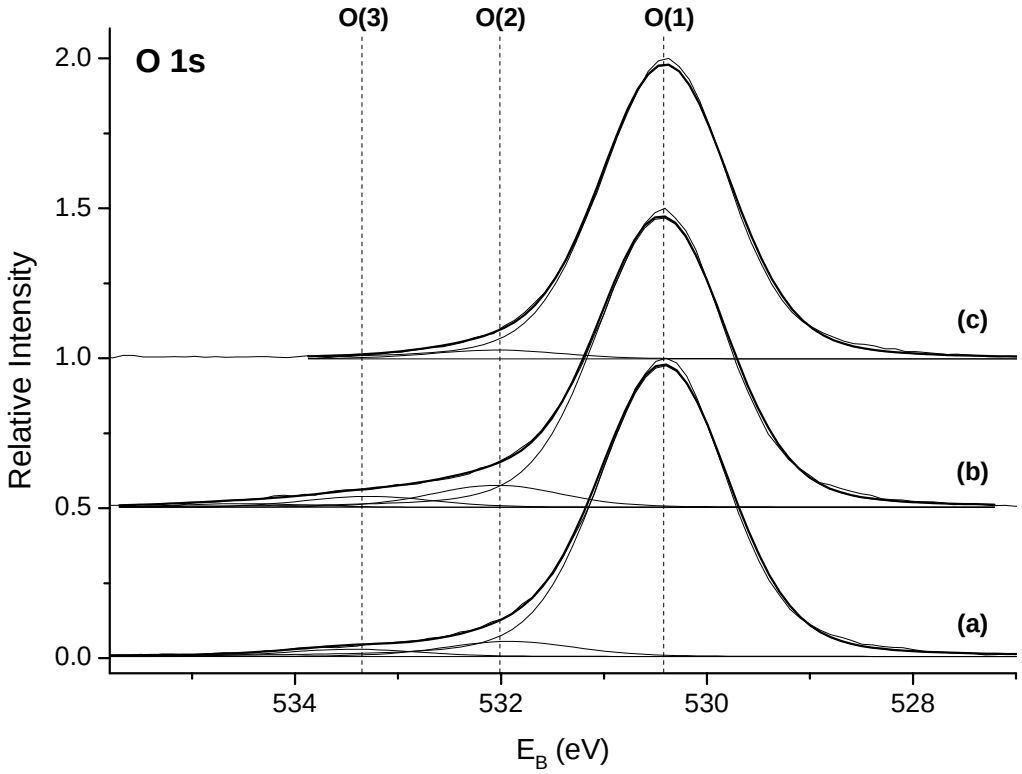

Figure 4.11: O 1s spectra of the thermal TiNb oxide before (a) and after H_2O treatment (b) and after TDS (c).

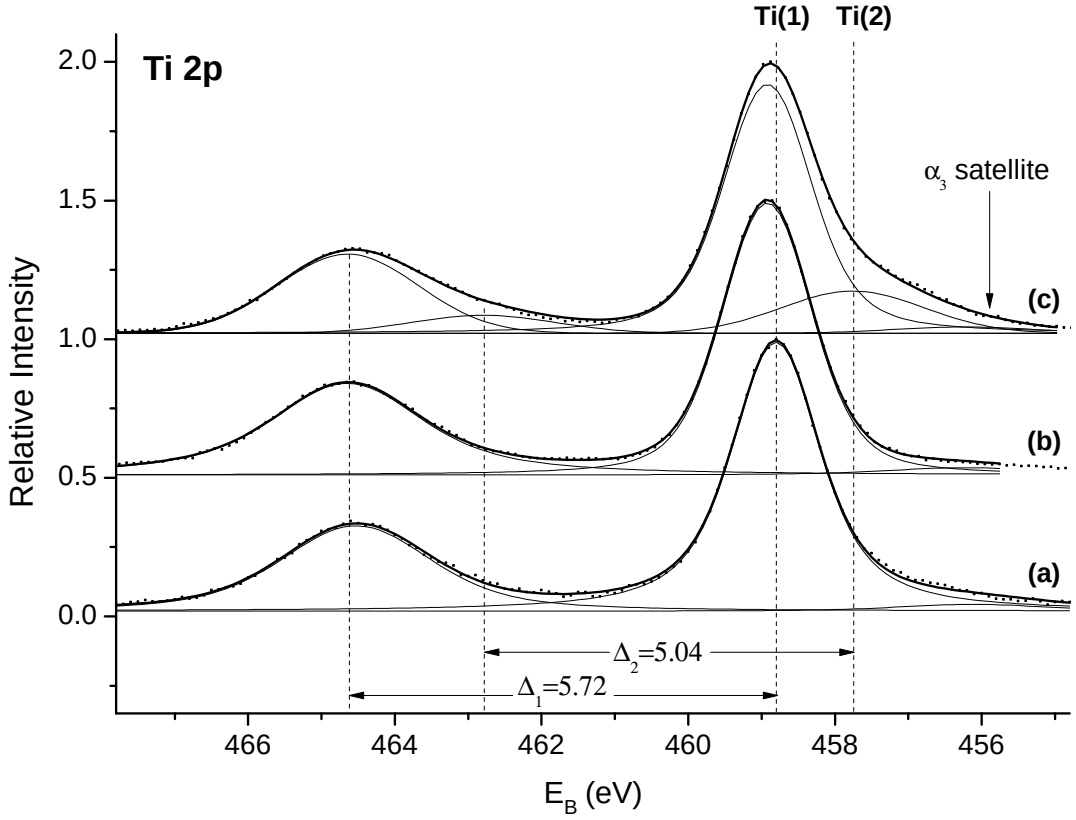

Figure 4.12: Ti 2p spectra of the natural TiNb oxide before (a) and after NaOH treatment (b) and after TDS (c).

sample surface, see Table 4.1. The C 1s line depicted in Figure 4.10 consists of C(1), C(2) and C(3) connected with graphite, CO and C=O, respectively. The H_2O treatment causes the modest increase of C 1s line and the TDS decreases the intensity lower than intensity of the spectra before treatment. That corresponds to the surface C concentration 19% and 9%. Relative intensities do not shows significant changes.

The O 1s line is shown in Figure 4.11. The dominant peak of O 1s line is O(1) attributed to the TiO_2 and Nb_2O_5 oxides. Besides this peak, two others at higher binding energies are observed, O(2) and O(3). The former one is assigned to OH groups and C=O groups and the latter one to O-C groups and chemisorbed water. After the sample boiling in water, the relative intensities of O(2) and O(3) increase. TDS decreases the relative intensity of smaller peaks.

4.1.4 NaOH treatment of a natural oxide

The Nb 3d spectra in Figure 4.1 (3a, 3b, 3c) show that Nb stays in the same oxidation state (Nb_2O_5). According to the Ti 2p spectra, titanium is in TiO_2 before and after NaOH treatment. After TDS, the majority of Ti is still in a form of TiO_2 and a part of it is in a Ti_2O_3 form as shown in Figure 4.12. The comparison of Ti/Nb ratio indicates that there is more titanium at the surface than before the NaOH soaking. The TDS decreases the ratio but it is still higher than the value before NaOH treatment.

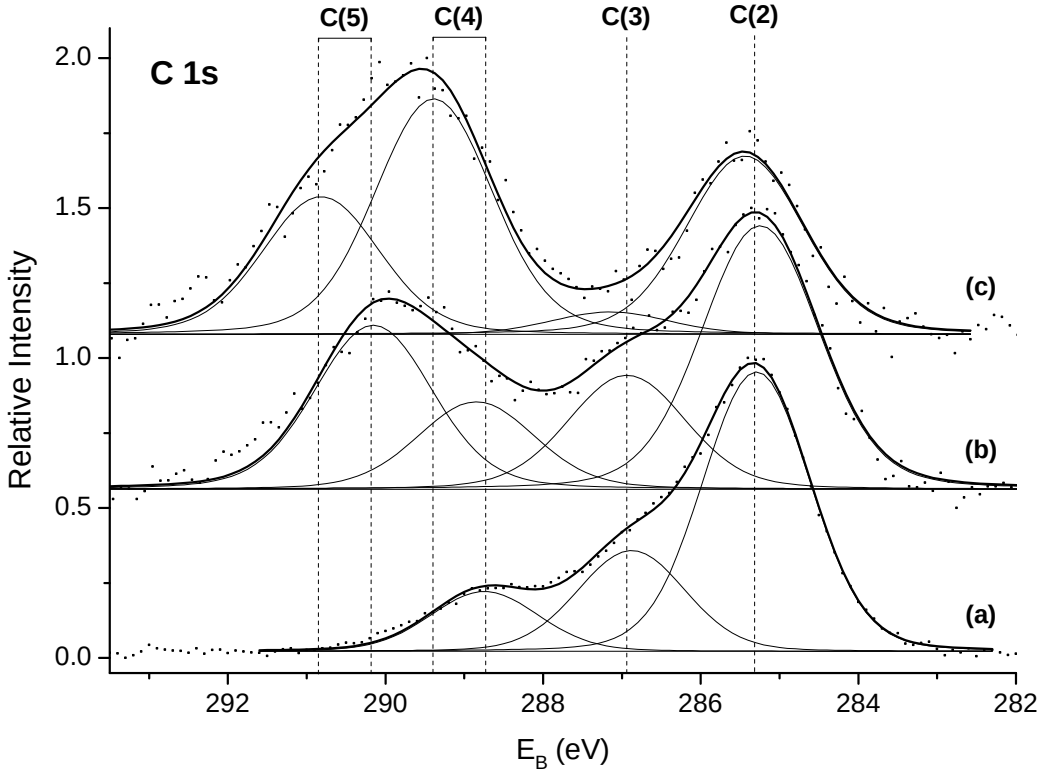

Figure 4.13: C 1s spectra of the natural TiNb oxide before (a) and after NaOH treatment (b) and after TDS (c).

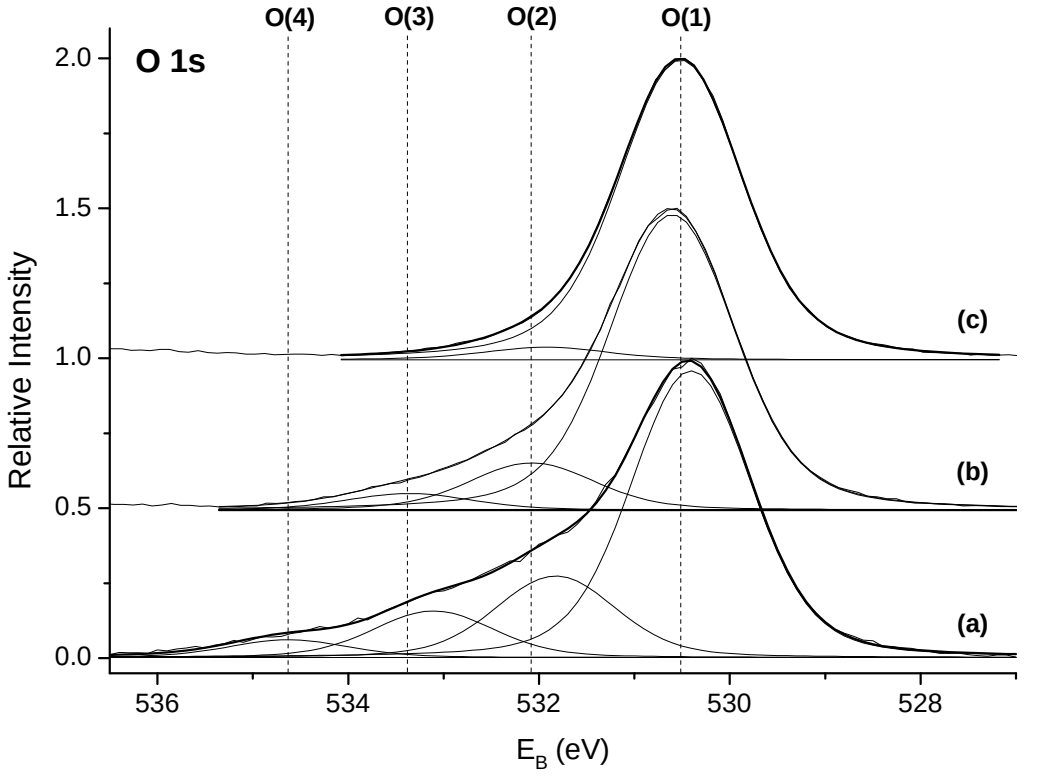

Figure 4.14: O 1s spectra of the natural TiNb oxide before (a) and after NaOH treatment (b) and after TDS (c).

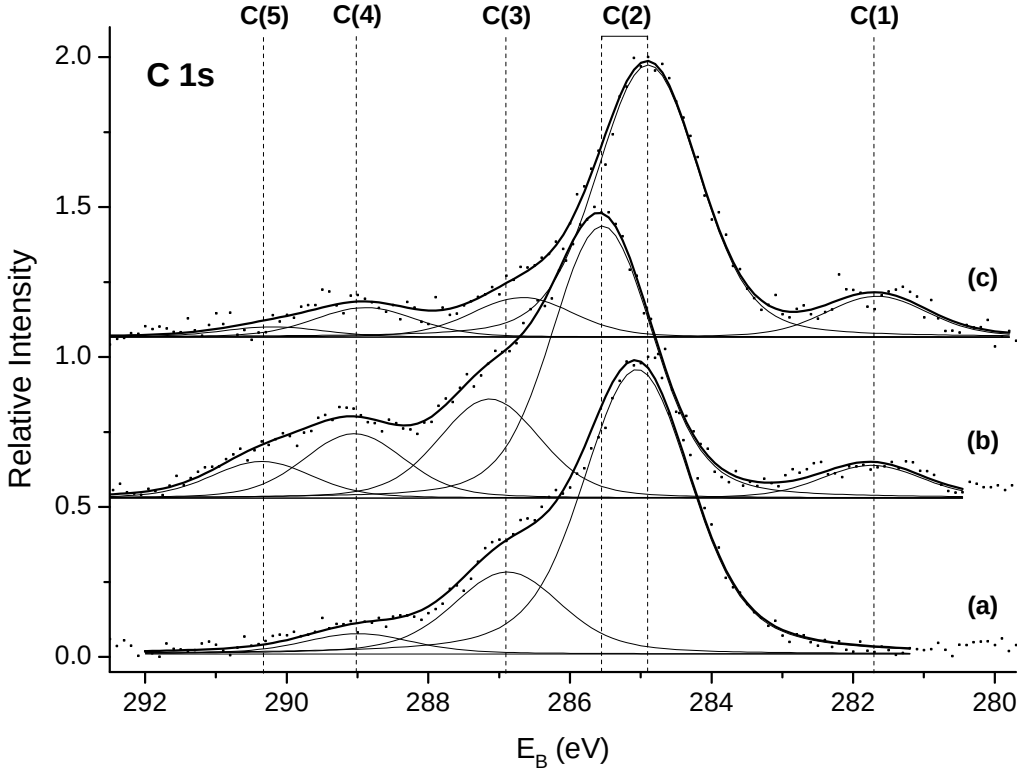

Figure 4.15: C 1s spectra of the thermal TiNb oxide before (a) and after NaOH treatment (b) and after TDS (c).

After polishing, there is 28% of C at the surface consisted of mostly graphite denoted by C(2). Peaks at higher binding energies are observed, C(3) and C(4) in Figure 4.13. The former one is assigned to C-O groups and the latter one to C=O groups. After the NaOH immersion, the graphite peak is significantly reduced while a new peak at higher energy C(5) appears. Following TDS causes more reduction of graphite and C-O peaks while the intensity of the high energy peak C(5) is increased. Due to the significant graphite peak reduction, the overall intensity is decreased and the C concentration is 17% (after NaOH soaking) and 10% (after TDS).

Before the NaOH treatment, the O 1s line is created by peaks denoted by O(1), O(2), O(3) and O(4) as shown in Figure 4.14. The NaOH soaking decrease the relative intensity of O(2), O(3) and O(4). After TDS, only O(1) and O(2) peaks left. The decreasing of intensities of peaks O(2), O(3) and O(4) is most likely connected with the decreasing intensity of carboneus contamination.

4.1.5 NaOH treatment of a thermal oxide

Ti and Nb do not change after the NaOH immersion and after TDS, depicted in Figures 4.3 and 4.1 (4a, 4b, 4c). They are in highly oxidized states corresponding to TiO_2 and Nb_2O_5. The Ti/Nb ratio could be taken as constant and with respect to deviations it corresponds to the preparation ration, Figure 4.5.

C 1s spectra are shown in Figure 4.15. As in case of natural oxide, the C(5) peak at higher energy appears after NaOH treatment and the intensity C(4) is

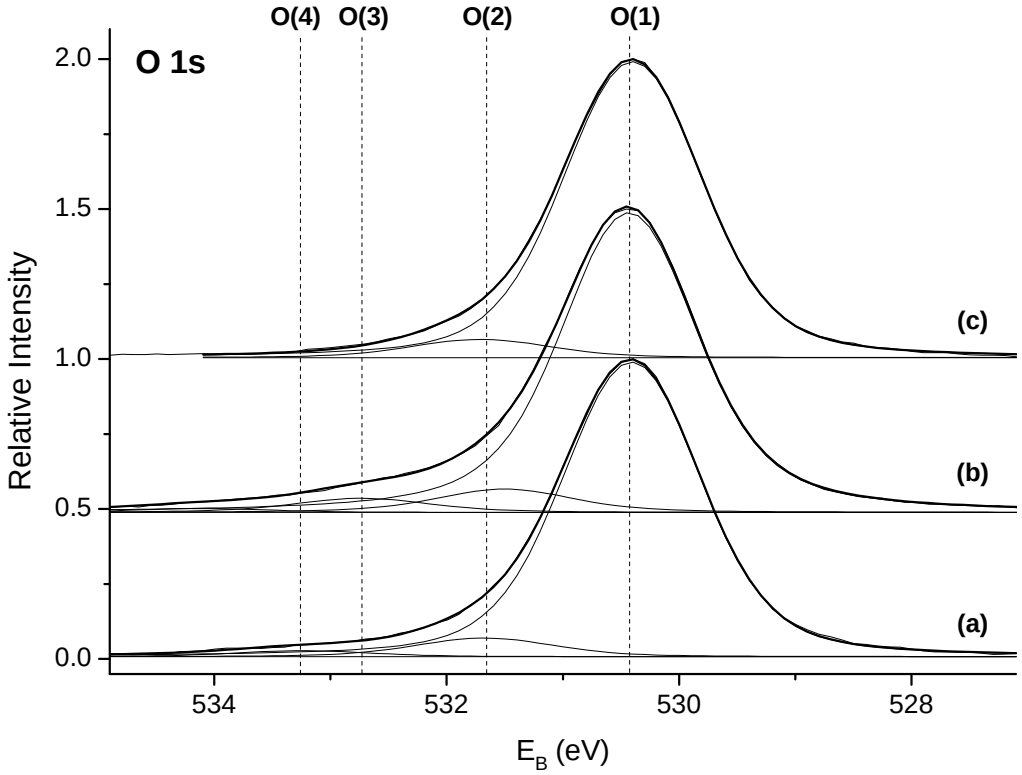

Figure 4.16: O 1s spectra of the thermal TiNb oxide before (a) and after NaOH treatment (b) and after TDS (c).

significantly increased. However, the carbide peak C(1) is created. TDS causes a reduction of the intensity except for the carbide peak which remains without changes. The overall concentration of carbon at the surface is before NaOH treatment 13%, after that 14% and after TDS it is decreased to 7% (Table 4.1).

In O 1s line shown in Figure 4.16, there is a dominant O(1) peak attributed to oxidized Ti and Nb. After NaOH soaking, the peak denoted by O(3) slightly grows. This peak is attributed to O-C groups and its increasing intensity correlate with increasing intensity of C-O peak C(3). After TDS, only the O(1) and O(2) peaks remain. That indicates the desorption or dissociation of oxygen components with higher binding energy.

4.2 RAIRS measurements

The infrared spectra are depicted in Figure 4.17. There are three spectra denoted by (a), (b) and (c) corresponding to the natural and thermal oxides measured after their preparation and thermal oxide after NaOH treatment, respectively. The spectrum of the natural oxide (a) uses as a reference the spectrum of the same sample after TDS. For (b) and (c) thermal oxide samples, the untreated thermal oxide after thermodesorption (TDS) is used as a reference.

We could understand a positive peak in Figure 4.17 as created groups (after TDS) while a negative peak indicates the desorption or dissociation of groups at sample. Each peak is connected to a relative change of amount of a corresponding group.

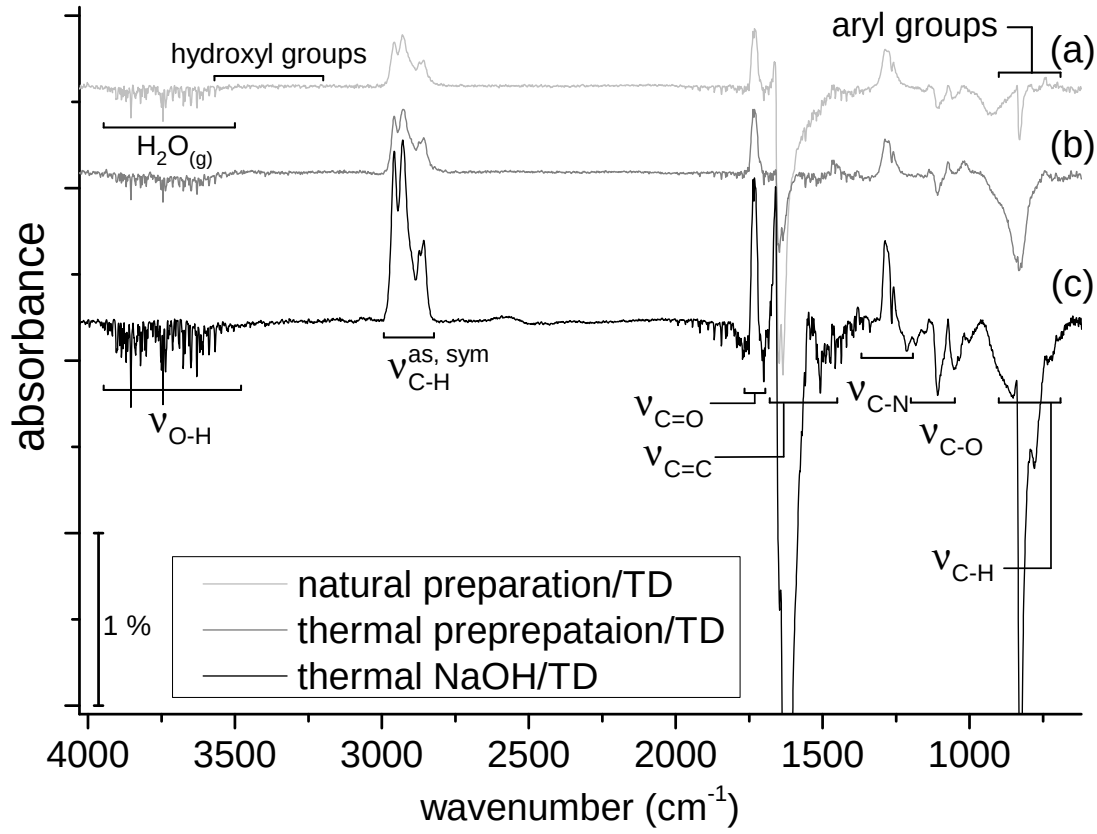

Figure 4.17: An infrared spectrum of natural oxide after the preparation (a) with TDS of natural oxide as a reference spectrum. Spectra of thermal oxide (b) after its preparation and thermal oxide treated with NaOH (c). As a reference of (b) and (c), it is used a measurement of untreated thermal oxide after thermodesorption.

The vibrations denoted by ν_{O-H} at energy ∼4000-3500 cm^{-1} corresponds to the O-H stretching. It is a characteristic range for vibrations of gaseous H_2O molecules. The desorption peaks are probably caused by H_2O molecules in a residual atmosphere due to the different level of evacuation during the sample and the reference measurements. The hydroxy O-H groups should be at energy of 3600-3200 cm^{-1} [19]. The OH groups bonded to the TiNb surface would occur at lower frequencies than the water region. There is no significant peak with respect to the intensities of peaks in the 4000-3500 cm^{-1} region.

The groups at 2800-3000 are assigned by $\nu^{as,sym}_{C-H}$. The maxima at energies of 2959 and 2873 cm^{-1} are attributed to methyl (-CH_3) asymmetric and symmetric stretch, respectively. The maxima at energies of 2930 and 2857 cm^{-1} are assigned to methylene (>CH_2) asymmetric and symmetric stretch, respectively [19]. Smaller positive peaks at 1468 (CH_2 bend) and 1462 cm^{-1} (CH_3 bend) were recognized. The shape of C-H stretch can be explained by a decomposition of hydrocarbons to more simply ones (containing CH_3-, -CH_2-).

The positive peak at energy of 1736 cm^{-1} denoted by $\nu_{C=O}$ is attributed to carbonyl group (C=O) vibrations [19]. The presence of this group corresponds to XPS measurements.

The intensive absorption peaks at 1680-1450 cm^{-1} are assigned to C=C groups

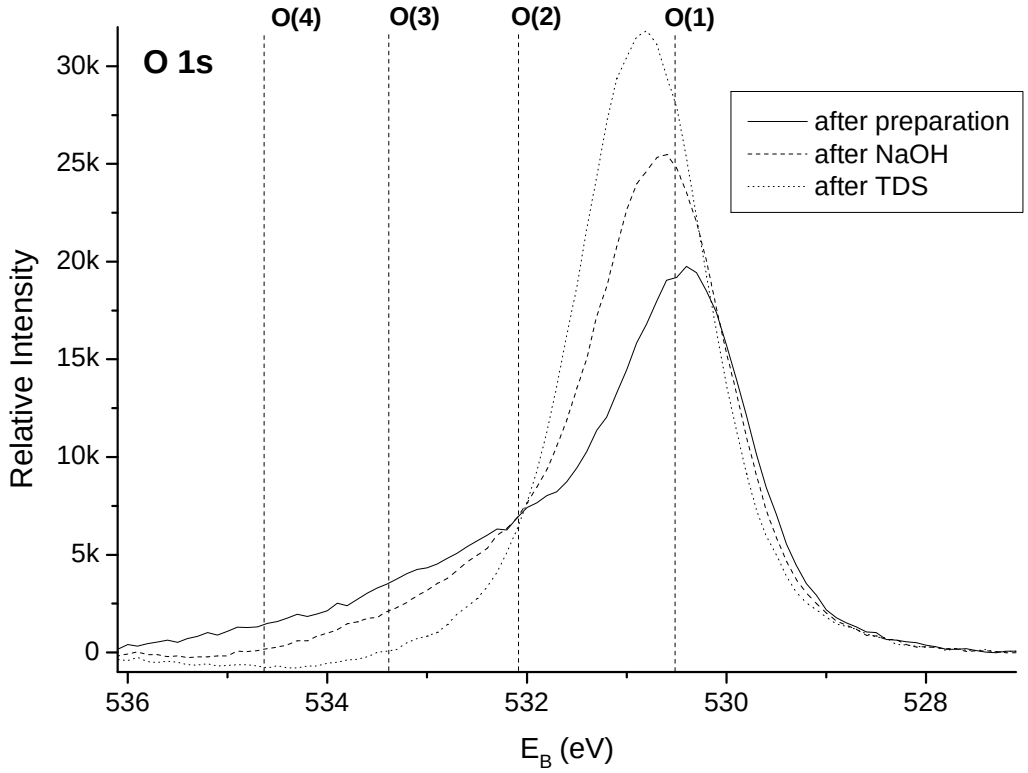

Figure 4.18: O 1s spectra of the natural TiNb oxide before (the solid line) and after NaOH treatment (the dashed line) and after TDS (the dotted line).

[19]. The samples after preparation contain peaks at positions 1648 and 1635 cm^{-1}. The NaOH treated sample includes additional energy of 1624 cm^{-1} which might be connected to aromatic hydrocarbons.

The peak in region from 1350 to 1260 cm^{-1} are designated by ν_{C-N}. Its frequency corresponds to nitrogen compounds (C-N).

Several ν_{C-O} frequencies can be observed at 1045, 1109, 1150, 1185, 1214, which could be attributed to C-O stretch of different kinds of alcohol molecules.

In Figure 4.17, there are significant desorption peaks with frequencies at 851, 825 and 780 cm^{-1} denoted by ν_{C-H} groups and they might be connected to the aryl functional group.

The all acquired spectra are very similar (Figure 4.17) which suggests that no visible changes between investigated samples. The RAIRS spectra show several means of carboneous contamination. Only small amount of peaks is positive which implies that the amount of the carboneous species after thermodesorption is lower.

4.3 OH groups

The OH groups bonded with Ti or Nb atoms should appear as a peak in O 1s spectra at higher position than O corresponding to the Ti and Nb oxides. That peak was designated by O(2) (all O 1s spectra are shown in Figure 4.2). The same binding energy is also attributed to O=C groups. The intensity of O(2) peak is too low for detailed quantitative analysis which could lead to separate of

the OH and O=C component. To the O 1s O=C peak, there are corresponding peaks in C 1s spectra (Figure 4.4) denoted by C(4). However, this peak is present for most of the acquired spectra. After the separation of OH peak from O(2) in O 1s line, the amount of OH groups bonded to C should be subtracted. C-OH groups have corresponding peak C(3) in C 1s line. This peak is present in all acquired spectra. Due to the low intensity of possible OH group peak in O(2) after subtraction C=O and C-OH peaks the resulting value would be negligible with respect to the deviation of XPS quantitative analysis. Nevertheless, the obvious changes in O(2) are observed. The changes in O 1s line are depicted in Figure 4.18. There is no normalization of intensity used.

IR spectroscopy does not prove OH bonded to the TiNb surface. Several O-H bonds were observed. However, they are attributed to water, alcohols and other carboneous species and water from residual atmosphere.

5. Conclusion

The surface of thermally prepared and naturally oxidized TiNb alloy samples is covered by TiO_2 and Nb_2O_5. The thermal oxide is more stable and remains in its oxidation state during H_2O, NaOH treatments and thermodesorptions. It is probably caused by the relatively thick layer of oxidized material. The significant reduction of Ti and Nb is observed when the naturally oxidized sample is treated with water and heated. However, a contribution of H_2O treatment is debatable because no changes after the treatment itself are observed. Small reduction of Ti and Nb at the surface of NaOH treated natural oxide also appears after thermodesorption.

The presence of OH^- groups bonded with the TiNb alloy was not proved. Although the binding energy of oxygen corresponding to the OH^- groups were found, it could not be attributed solely to these groups.

The further investigation of TiNb alloy is required. Considering the titanium and niobium reactivity, it is possible that the surface is saturated with air CO and H_2O and does not have any response to the H_2O treatment. Therefore, model studies under the UHV conditions are proposed, i.e., H_2O adsorptions at defined surfaces. In order to determine H_2O treatment influence before thermodesorption, it is suggested to perform a thermodesorption of untreated samples which was not measured because of time and material requirements. Possible future experiments could include immersion in SBF (simulated body fluid) and subsequent apatite growth observation.

Bibliography

[1] David F Williams. On the mechanisms of biocompatibility. *Biomaterials*, 29(20):2941–2953, 2008.

[2] Hiroaki Takadama, Hyun-Min Kim, Tadashi Kokubo, and Takashi Nakamura. Xps study of the process of apatite formation on bioactive ti–6al–4v alloy in simulated body fluid. *Science and Technology of Advanced Materials*, 2(2):389–396, 2001.

[3] David G Castner and Buddy D Ratner. Biomedical surface science: Foundations to frontiers. *Surface Science*, 500(1):28–60, 2002.

[4] James M Anderson. Biological responses to materials. *Annual Review of Materials Research*, 31(1):81–110, 2001.

[5] Matthew Tirrell, Efrosini Kokkoli, and Markus Biesalski. The role of surface science in bioengineered materials. *Surface Science*, 500(1):61–83, 2002.

[6] Yikai Chen, Xuebin Zheng, Heng Ji, and Chuanxian Ding. Effect of ti–oh formation on bioactivity of vacuum plasma sprayed titanium coating after chemical treatment. *Surface and Coatings Technology*, 202(3):494–498, 2007.

[7] Xuanyong Liu, Paul K Chu, and Chuanxian Ding. Surface modification of titanium, titanium alloys, and related materials for biomedical applications. *Materials Science and Engineering: R: Reports*, 47(3):49–121, 2004.

[8] Jonathan Black. Does corrosion matter? *Journal of Bone & Joint Surgery, British Volume*, 70(4):517–520, 1988.

[9] M A Khan, Rachel L Williams, and David F Williams. The corrosion behaviour of ti–6al–4v, ti–6al–7nb and ti–13nb–13zr in protein solutions. *Biomaterials*, 20(7):631–637, 1999.

[10] Alessandra Cremasco, Wislei R Osorio, Célia MA Freire, Amauri Garcia, and Rubens Caram. Electrochemical corrosion behavior of a ti–35nb alloy for medical prostheses. *Electrochimica Acta*, 53(14):4867–4874, 2008.

[11] Daniel P Perl and Arnold R Brody. Alzheimer's disease: X-ray spectrometric evidence of aluminum accumulation in neurofibrillary tangle-bearing neurons. *Science*, 208(4441):297–299, 1980.

[12] Ivan Jirka, Marta Vandrovcová, Otakar Frank, Zdeněk Tolde, Jan Plšek, Thomas Luxbacher, Lucie Bačáková, and Vladimír Starý. On the role of nb-related sites of an oxidized β-tinb alloy surface in its interaction with osteoblast-like mg-63 cells. *Materials Sccastner2002biomedicalience and Engineering: C*, 33(3):1636–1645, 2013.

[13] Lidia Benea, Eliza Mardare-Danaila, Marilena Mardare, and Jean-Pierre Celis. Preparation of titanium oxide and hydroxyapatite on ti–6al–4v alloy surface and electrochemical behaviour in bio-simulated fluid solution. *Corrosion Science*, 80:331–338, 2014.

[14] Gerhard Ertl and Jürgen Küppers. *Low energy electrons and surface chemistry*. Vch Weinheim, 1985.

[15] David Briggs and John T Grant. *Surface analysis by Auger and X-ray photoelectron spectroscopy*. IM Publications, 2003.

[16] Peter Hollins. The influence of surface defects on the infrared spectra of adsorbed species. *Surface Science Reports*, 16(2):51–94, 1992.

[17] R Raval. Probing the nature of molecular chemisorption using rairs. *Surface science*, 331:1–10, 1995.

[18] Michael Trenary. Reflection absorption infrared spectroscopy and the structure of molecular adsorbates on metal surfaces. *Annual review of physical chemistry*, 51(1):381–403, 2000.

[19] John Coates. Interpretation of infrared spectra, a practical approach. *Encyclopedia of analytical chemistry*, 2000.

[20] Yves J Chabal. Surface infrared spectroscopy. *Surface Science Reports*, 8(5):211–357, 1988.

[21] Petr Janeček. *Diploma thesis*. MFF UK, 2001.

[22] Rudolf Plank. *VERTEX 70v User Manual*. BRUKER OPTIK GmbH, 2007.

[23] Jonhn F Moulder, William F Stickle, Peter E Sobol, and Kenneth D Bomben. *Handbook of X-ray Photoelectron Spectroscopy*. Physical Electronics, 1995.

[24] Carine Viornery, Yann Chevolot, Didier Léonard, Björn-Owe Aronsson, Péter Péchy, Hans Jörg Mathieu, Pierre Descouts, and Michael Grätzel. Surface modification of titanium with phosphonic acid to improve bone bonding: characterization by xps and tof-sims. *Langmuir*, 18(7):2582–2589, 2002.

[25] Victor V Atuchin, Valery G Kesler, Natalia V Pervukhina, and Zhaoming Zhang. Ti 2p and o 1s core levels and chemical bonding in titanium-bearing oxides. *Journal of electron spectroscopy and related phenomena*, 152(1):18–24, 2006.

[26] J Pouilleau, D Devilliers, Henri Groult, and P Marcus. Surface study of a titanium-based ceramic electrode material by x-ray photoelectron spectroscopy. *Journal of materials science*, 32(21):5645–5651, 1997.

[27] A A Voevodin, M A Capano, S J P Laube, M S Donley, and J S Zabinski. Design of a ti/tic/dlc functionally gradient coating based on studies of structural transitions in ti–c thin films. *Thin Solid Films*, 298(1):107–115, 1997.

[28] James E Krzanowski and Robert E Leuchtner. Chemical, mechanical, and tribological properties of pulsed-laser-deposited titanium carbide and vanadium carbide. *Journal of the American Ceramic Society*, 80(5):1277–1280, 1997.

[29] Yu-Hsu Chang and Hsin-Tien Chiu. Nano-sizing titanium into titanium carbide by 1-chlorobutane. *Journal of Materials Research*, 17(11):2779–2782, 2002.

[30] V L S Teixeira Da Silva, M Schmal, and S T Oyama. Niobium carbide synthesis from niobium oxide: study of the synthesis conditions, kinetics, and solid-state transformation mechanism. *Journal of Solid State Chemistry*, 123(1):168–182, 1996.

[31] Henriette Estrade-Szwarckopf. Xps photoemission in carbonaceous materials: a "defect" peak beside the graphitic asymmetric peak. *Carbon*, 42(8):1713–1721, 2004.

[32] Jukka Lausmaa. Surface spectroscopic characterization of titanium implant materials. *Journal of Electron Spectroscopy and Related Phenomena*, 81(3):343–361, 1996.

[33] Erika E Johnston and Buddy D Ratner. Surface characterization of plasma deposited organic thin films. *Journal of electron spectroscopy and related phenomena*, 81(3):303–317, 1996.

[34] R A Zarate, S Fuentes, Juan P Wiff, V M Fuenzalida, and A L Cabrera. Chemical composition and phase identification of sodium titanate nanostructures grown from titania by hydrothermal processing. *Journal of Physics and Chemistry of Solids*, 68(4):628–637, 2007.